Master Thesis

Entitled

The Role of Autophagy in Shaping Inhibitory Synapses

Neurophagy lab

Supervisor: Dr. Vassiliki Nikoletopoulou

Anastasios Kollias

Molecular Biology and Biomedicine

Department of Biology

University of Crete

Greece

10/2018

Table of Contents

Abstract 3
A. Introduction 4
A.1 Autophagy 4
A.1.2. Molecular mechanisms of autophagy 5
A.1.3 Regulation of autophagy…..... 6
A.1.4 Autophagy in the Central Nervous System (CNS)..... 8
A.1.4.2 Autophagy at the synapses ……..... 9
A.2 Brain inhibition ……..... 11
A.2.2. Different migratory routes between excitatory an inhibitory neuronal populations..... 12
A.2.2.1 Medial Ganglionic Eminence..... 12
A.2.2.2 *Lhx6*+ subclasses of interneurons…….... 13
A.2.3. Inhibitory plasticity – E/I balance..... 16
B. Aim of the study..... 18
C. Results 19
C.1. A model for ablation of autophagy in inhibitory neurons: Construction of mice with conditional ablation of *Atg5* in MGE-derived interneurons. 19
C.2. *In vitro* primary neuronal cultures indicate increased cell body size and number of primary dendrites in c*Atg5*KO compared to control……..... 20
C.3. *In vivo* experiments demonstrating increased inhibitory markers, reduced spines and LTP deficits and in c*Atg5*KO animals……..…….. 20
C.4. Behavioral characterization of c*Atg5*KO animals demonstrating memory deficits, resistance to seizures and general anxious-like behavior. 24
C.5 Construction of a new mouse model that *Atg5* is ablated in the majority of pyramidal neurons in different time periods (p15-pups or p60-adult)..... 26
D. Discussion and future plans 28
D.1. Does autophagy deficiency in interneurons result in increased brain inhibition?.... 30
D.2. Generation of double-cre autophagy deficient mice ……..…..33
E. Methods..... 33
E.1. Mice 33
E.2. Genotyping ……..34
E.3. Western blot 34
E.4. Immunohistochemistry – Immunofluorescence…….. 35
E.5. Neuronal cultures …. 35
E.6. Immunostaining…….. 36
E.7. Golgi staining …….. 36
E.8. Anxiety-related tests ……37
E.9 Contextual Fear Conditioning…….…….…….. 38
E.10. Pilocarpine model ……..38
E.11. Electrophysiology ……..…….39
E.12. Quantification and statistical analysis ……40
F. Bibliography 41

Abstract

Macroautophagy is a highly conserved multistep process that sequesters cellular constituents in autophagic vesicles and delivers them to the lysosome for degradation. Though initially considered as a process in bulk, it is increasingly appreciated that autophagy can serve specific functions in specialized cell types. In line with this notion, recent evidence suggests that autophagy is modulated by neuronal activity in glutamatergic hippocampal neurons and that its ablation in excitatory neurons results in autistic-like behaviors due to aberrant developmental spine pruning, a process known to be mediated by LTD-like mechanisms. As excitatory neurons represent the vast majority in the forebrain and synaptic plasticity traditionally studied in these cells has been shown to underlie key cognitive functions such as memory and learning, work so far has focused on delineating the role of autophagy in excitatory neurons, ignoring the minority interneuron populations responsible for brain inhibition. We characterized the role of autophagy in shaping inhibitory synapses by generating the first knockout mice with conditional deletion of *Atg5*, a gene that is required for autophagy, in interneurons derived from the medial ganglionic eminence (MGE). Our findings suggest that autophagy has a crucial role in dictating brain inhibition, as autophagy-deficiency in GABAergic neurons leads to increased inhibition and compromised synaptic plasticity and memory.

A. Introduction

A.1.1 What is autophagy?

Autophagy is a highly conserved catabolic pathway by which dysfunctional or superfluous damaged intracellular constituents are driven to the lysosomes for degradation. Autophagy runs in parallel to the Ubiquitin-Proteasome System (UPS), however it does not only degrade proteins but also other macromolecules and organelles, such as proteins, lipids, ribosomes, nuclei, endoplasmic reticulum (ER) and mitochondria. Therefore, autophagy is essential for the cell to produce new building blocks and safeguard its cellular homeostasis. Apart from its housekeeping role under basal conditions, under nutrient starvation, hypoxia or energy depletion, hormonal stimulation or pharmaceutical agents autophagy can also be increased in the cells in order to recycle cytosolic components and compensate for the negative energy equilibrium.

Three types of autophagy have been proposed: microautophagy, chaperone-mediated autophagy (CMA) and macroautophagy (Seglen and Bohley 1992). Microautophagy involves the direct engulfment of cytoplasmic cargo into the lysosome via invagination of the lysosomal membrane, while CMA involves the direct translocation of cytoplasmic proteins by HSC70 and its co-chaperones, that recognize cytosolic proteins with a KFERQ-like pentapeptide, to the lysosomal protein LAMP2A resulting in their unfolding and degradation.

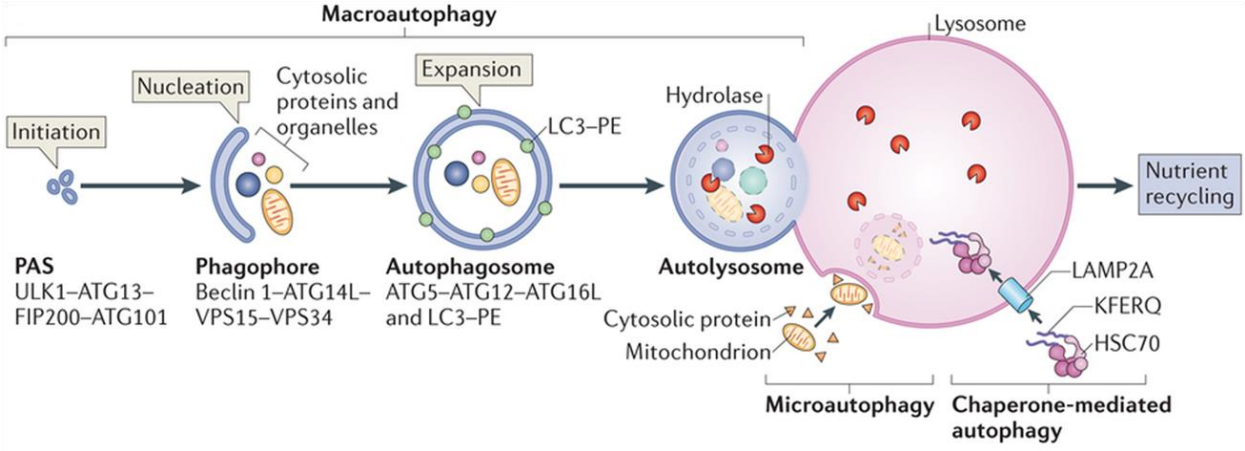

Figure 1. Different types of autophagy and the steps of molecular macroautophagic machinery (adapted from Kaur & Debnath, 2014).

Macroautophagy is the major (and most studied) type of autophagic process, whereby cargo is recognized and enclosed by an isolation membrane, which elongates and forms a double membrane structure, the autophagosome which fuses with the lysosome for degradation (Figure 1). (Mizushima and Komatsu 2011; Mizushima, Yoshimorim, and Levine 2010; V. Nikoletopoulou, Papandreou, and Tavernarakis 2015). Hereafter macroautophagy will be referred to as autophagy for convenience.

A.1.2. Molecular mechanisms of autophagy

Initiation

The molecular mechanism of autophagy involves several conserved autophagy–related (Atg) proteins. Autophagy starts with the formation of the pre-autophagosomal structure (PAS), a cup shaped membrane known as the phagophore derived from the ER. PAS components comprise the Ulk1 complex that is consisted of Ulk1, FIP200, ATG13 and ATG101. Their association is known to lead to proper localization of ULK1 and stimulate its kinase activity. The activated Ulk1 complex recruits the (Ptdlns)3-kinase complex (including Ambra1, Beclin 1, Atg14(L)/barkor, Vps15 and Vps34) to initiate the vesicle nucleation (Ganley et al. 2009).

Vesicle Nucleation and Elongation

Essential for vesicle nucleation are Double FYVE-containing protein 1 (DFCP1) and WD repeat domain phosphoinositide-interacting protein (WIPI), which form a specific ER structure, the omegasome that serves as a platform for the formation of the phagophore and the initiation of vesicle nucleation (K. H. Kim and Lee 2014). Phagophore elongation and autophagosome completion requires two ubiquitin–like conjugation pathways. The first leads to the conjugation of Atg5–Atg12 through the concerted action of ATG7 (E1-like enzyme) and ATG10 (E2-like enzyme), which then form a multimeric complex with Atg16L. The second ubiquitin–like system involved in autophagosome formation results in the processing of microtubule–associated protein light chain 3 (LC3-II). LC3-I, the cytosolic form of LC3 is generated by cleavage of pro-LC by ATG4B and further processed by ATG7 and ATG3 to form the PE-LC3 / LC3-II protein, a

species that integrates into lipid membranes of phagophores and autophagosomes and can directly interact with autophagic protein substrates through the LIR (LC3 interacting region) motif. After the closure of the autophagosome Atg16–Atg5–Atg12 complex dissociates from the autophagosome, but LC3B–II is found on both the inner and the outer surfaces of the autophagosome and its levels correlate with the number of autophagosomes, therefore, LC3-II is used as a marker of autophagy (Mizushima and Komatsu 2011; V. Nikoletopoulou, Papandreou, and Tavernarakis 2015).

Fusion with lysosome and degradation

Mature autophagosomes become fused with lysosomes to form autolysosomes. In the final step, cytoplasmic components are digested by lysosomal enzymes. In addition to the cargo, lysosomal enzymes also degrade the inner membrane of the autophagosome (V. Nikoletopoulou, Papandreou, and Tavernarakis 2015).

A.1.3 Regulation of autophagy

At the cellular level, autophagy is the primordial system for energy production and can be induced by starvation or limitation of nutrients, amino acids, glucose, growth factors, oxygen and energy or by many different types of stress. Availability of these factors activates the serine/threonine protein kinase mTORC1 (mammalian target of rapamycin complex 1) and autophagy is blocked (Figure 2). Briefly, there are three distinct signaling pathways converge on mTORC1 activation to inhibit autophagy; the Rag/mTORC1 pathway that senses availability of amino acids and nutrient sufficiency, the PI3KC1a/Akt/TSC/mTORC1 pathway that senses growth factors sufficiency and the AMPK/TSC/mTORC1 pathway that integrates intracellular stress signals and energy levels (Sarkar 2013). In general the mTOR pathway regulates vital cellular functions and when it is activated the mTORC1 phosphorylates the Ulk1 and ATG13 proteins, resulting in the inhibition of their kinase activity, therefore the PAS complex cannot be assembled (Jung et al. 2010).

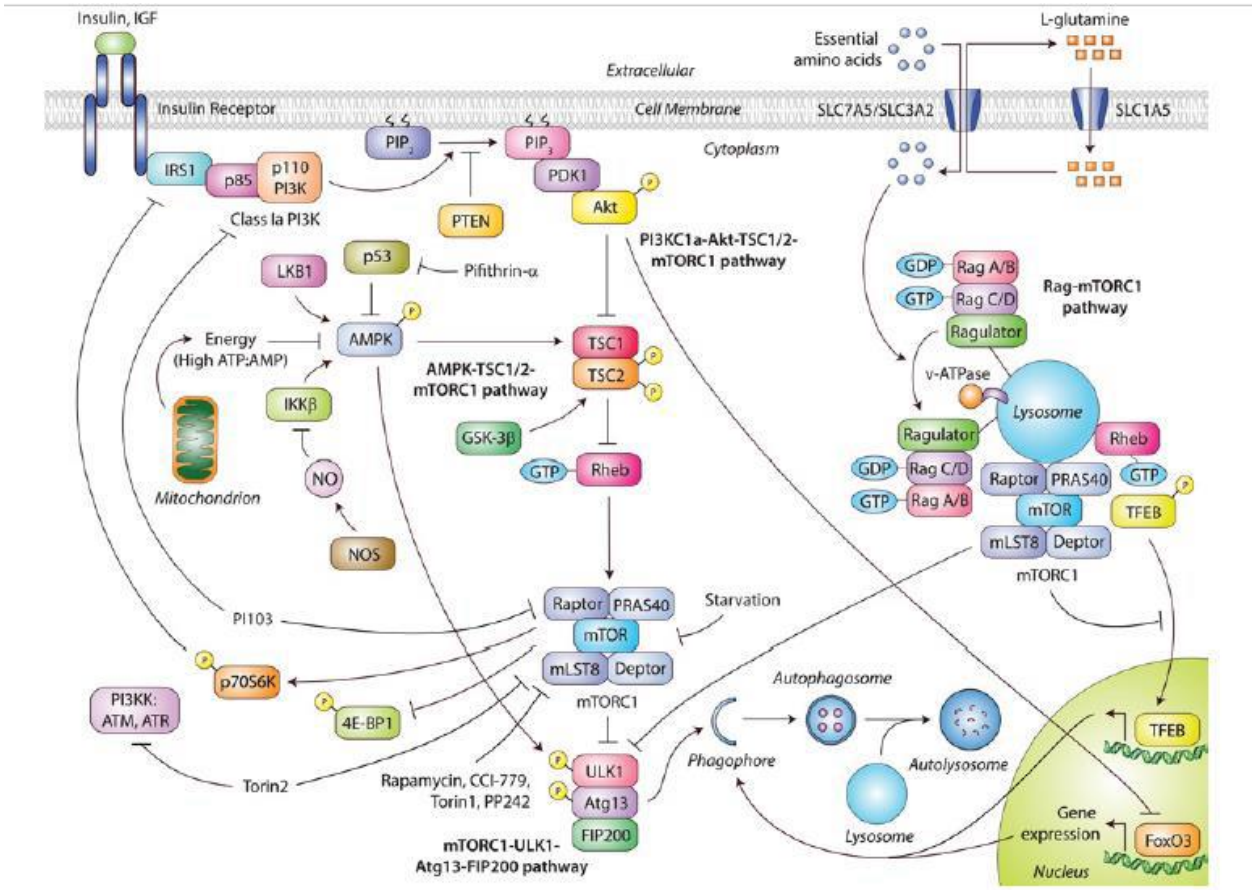

Figure 2. Regulation of autophagy by mTOR-dependent pathways. Note that when mTOR is active the formation of Ulk1 complex is inhibited and autophagy cannot be initiated (adapted from Sarkar, 2013)

Moreover, there are mTORC1-independent signaling pathways, like inositol signaling, the calcium/calpain pathway, the cAMP and the JNK signaling pathways that regulate autophagy in mTOR-independent manner, as they are presented in Figure 3. As far as the calcium/calpain pathway is concerned, the increase of intracellular calcium $[Ca^{2+}]i$ activates the cysteine proteases calpains which block the transition from phagophore to autophagosome, so autophagy is blocked (Sarkar 2013).

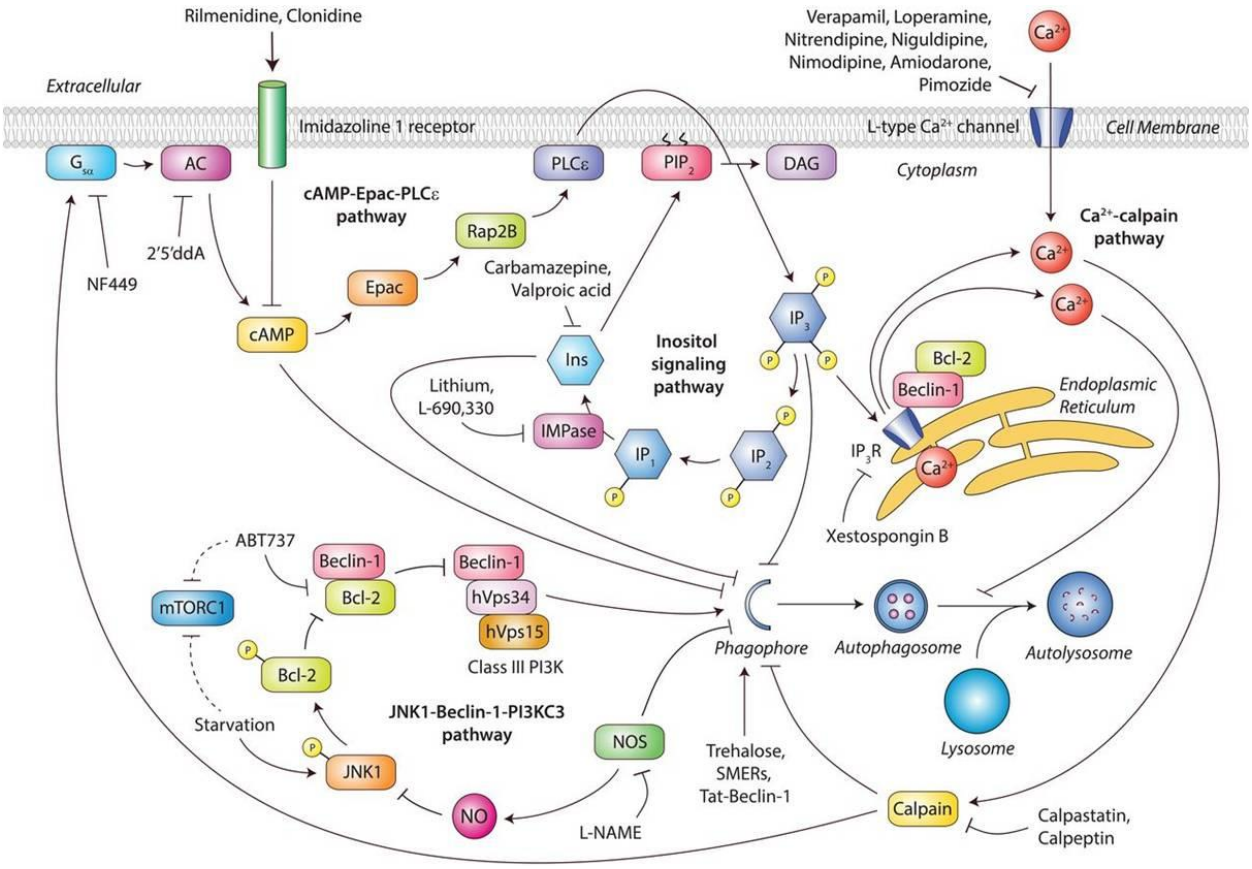

Figure 3. Regulation of autophagy by TOR-independent pathways (adapted from Sarkar, 2013)

A.1.4 Autophagy in the Central Nervous System (CNS)

It is increasingly appreciated that basal autophagy is indispensable for neuronal maintenance and quality control. Ablation of autophagy in the neural lineage leads to widespread neurodegeneration and progressive motor deficit, accompanied by accumulation of protein aggregates and reduction in the number of pyramidal neurons in the cerebral cortex and of Purkinje cells in the cerebellar cortex (Hara et al. 2006; Komatsu et al. 2006). However, it is difficult to infer which of these effects can be attributed to autophagy deficiency in neurons rather than glial cells.

A.1.4.2 Autophagy at the synapses

The synapse is a highly specialized neuronal structure that permits a neuron to pass an electrical or chemical signal to another neuron or to the target effector cell. On the one side, there is the presynaptic button that is packed with synaptic vesicles containing neurotransmitters and contains the machinery to release these vesicles into the synaptic cleft and retrieve back the fused vesicle membranes. On the other side, there is the postsynaptic density that contains high amount of receptors that can be activated by the released neurotransmitters, and other scaffold, cytoskeletal, and signalling molecules, to ensure the activation of the postsynaptic neuron. In the majority of neurons, especially the pyramidal ones, these postsynaptic densities are mostly located in the dendritic spines, outgrowths of dendritic shafts (Figure 4A) (Nikoletopoulou and Tavernarakis 2018). Spines are the most actin-rich dynamic structures in the brain and exist only on certain types of neurons, including pyramidal neurons in the cortex, medium spiny neurons in the basal ganglia and Purkinje cells in the cerebellum. Spines with strong synaptic contacts typically have a large spine head, which connects to the dendrite via a membranous neck. They can be categorized into three classes according to their shape as: thin, stubby and mushroom. (Figure 4B) (Rochefort and Konnerth 2012). Most of the times, dendritic spines exist in an immature transient nature, dendritic filopodia, that receive synaptic input, and can develop into dendritic spines due to the neuronal activity (Portera-Cailliau, Pan, and Yuste 2003).

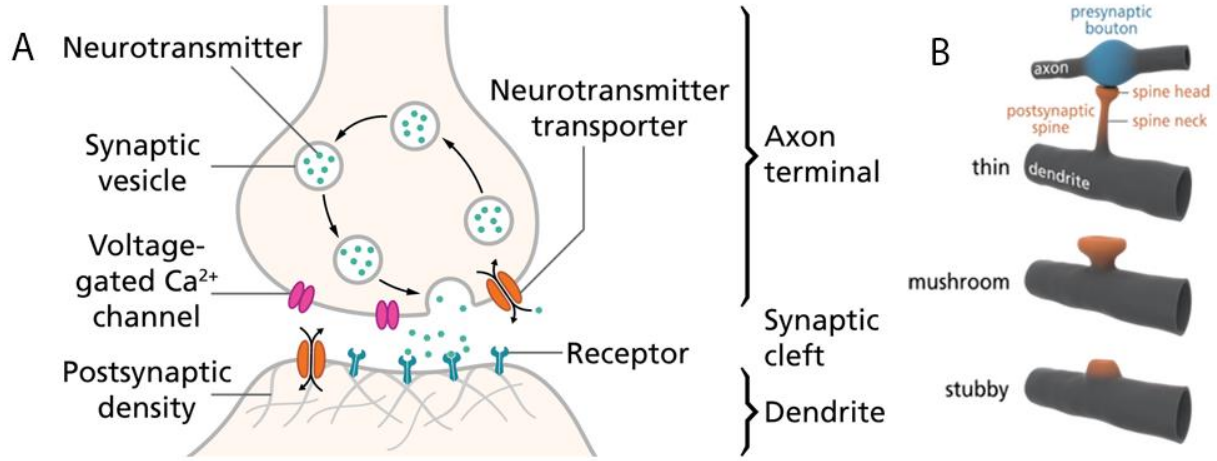

Figure 4. A) Schematic representation of a neuronal synapse. B) Distinct types of dendritic spines

Both forms of long synaptic plasticity in the mammalian brain, Long Term Potentiation (LTP) and Long Term Depression (LTD), are expressed by structural changes in the postsynaptic side with the enhancement or shrinkage of pre-existing dendritic spines. They both require protein turnover where it exists protein synthesis and degradation respectively (Alvarez-Castelao and Schuman 2015). The induction of LTP or LTD induces structural plasticity of spines in stimulated dendritic branches. The link between LTP and spine structure was suggested by the finding that the size of the postsynaptic density (PSD) is related to the size of the spine head and the number of AMPA-type glutamate receptors within it. (Kasai et al. 2010)

Recent work from our lab highlighted the role of BDNF, the major growth factor of the CNS, on the regulation of neuronal autophagy. Mature BDNF can block the transition of the phagophore to the autophagosome and by doing so, it allows synaptic proteins that are normally autophagic cargo to accumulate in the synapse and mediate the growth and addition of new spines that are required for LTP (Figure 5). In addition, the dynamic participation of autophagy in synapse remodeling was revealed by directly degrading key synaptic proteins (Nikoletopoulou et al. 2017) or induction of PAS components after induction of NMDAR- and mGluR- dependent LTD (Kallergi et al., submitted).

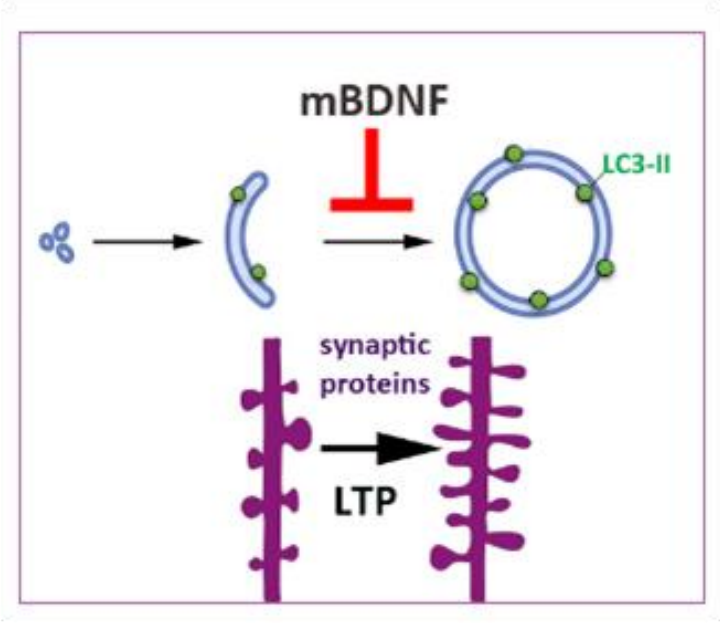

Figure 5. Mature BDNF blocks the transition from phagophore to autophagosome and synaptic proteins accumulate in the synapse and mediate the growth and addition of new spines that are required for LTP (adapted from Nikoletopoulou et al. 2017).

The role of autophagy in synaptic pruning, a critical period, between postnatal days 20 and 30 in mice, where excess dendritic spines in the cortex are eliminated, was emphasized when autophagy was ablated in forebrain excitatory neurons (*CamkII-Cre;Atg7flox/flox* mice) during this period. These mice exhibit autistic-like cognitive and social deficits but most important increased number of spines after the pruning period because of defective LTD-like mechanisms (Tang et al. 2014). Interestingly, conditional

ablation of autophagy in microglia, a representative immune cell in the brain, also impairs synaptic pruning in a similar way, demonstrating increased number of spines even before pruning and behavioral deficits (impaired sociability, repetitive behavior) associated with Autism Spectrum Diseases (ASD), a range of neurodevelopmental disorders that includes autism and related conditions, at adult age. (H. J. Kim et al. 2017)

Synaptic plasticity has been traditionally studied in the excitatory neurons since they represent the vast majority in the forebrain ignoring the minority of interneuron populations that are responsible for the brain inhibition.

A.2.1 Brain inhibition

Interneurons constitute a highly heterogeneous group of neurons that can be grouped according to their morphological, electrophysiological and molecular features as well as their connectivity and origin. They stabilize the neuronal networks through synaptic inhibition and modulate network activity by shaping the spatiotemporal dynamics of different forms of synchronized oscillations. All these properties affect their responses to excitatory inputs and their postsynaptic impact onto target cells. They also vary in their response to neuromodulators such as acetylcholine (Ach), serotonin (5-HT), noradrenaline, dopamine and their expression of molecules such as calcium-binding proteins [e.g. parvalbumin (PV), calretinin (CR) and calbindin (CB)] and neuropeptides [e.g. Neuropeptide Y (NPY)]. Most interneurons (or local circuit neurons, LCNs), primarily use the neurotransmitter GABA (g-aminobutyric acid) and they comprise only 10–15% of the entire neuron population but play crucial roles in regulating neuronal excitability, since they stabilize the excitation to inhibition ratio (E/I balance) to help maintain neuronal activity within a narrow, safe range. Specific interneuron subtypes are implicated in regulating neuronal proliferation and migration as well as postnatal maturation of cortical circuitry. Malfunction of inhibitory INs has been associated with the generation of several types of epilepsy, schizophrenia, anxiety disorders and autism (Ascoli et al. 2008; Klausberger and Somogyi 2008; Tremblay, Lee, and Rudy 2017).

A.2.2. Different migratory routes between excitatory an inhibitory neuronal populations

Even though it was widely assumed that the excitatory and inhibitory neurons within the cortex shared a common lineage it is now accepted that excitatory and inhibitory neurons are originated from different subcortical developmental domains, the pallium and the subpallium respectively. The subpallium gives rice to two major areas: the medial ganglionic eminence (MGE) and the caudal ganglionic eminence (CGE) and two complementary areas: the lateral ganglionic eminence (LGE) and the preoptic area (POA) each one giving rise to distinct interneuron subtypes (Figure 6). Briefly, the MGE gives rise to the parvalbumin (PV)-expressing fast spiking interneurons (including both basket and chandelier cells), the somatostatin (SST)-expressing populations, of which the Martinotti cells form the largest subset and the nitric oxide synthase (nNOs) early in development. The CGE generates a remarkable diversity of LCN subclasses, variably overlapping, based on their expression of calretinin, vasoactive intestinal protein (VIP), reelin, and Neuropeptide Y. (Chu and Anderson 2015)

Like their neocortical counterparts, hippocampal interneurons arise from medial and caudal ganglionic eminence (MGE and CGE) precursors but are produced in two neurogenic waves between E9–12 and E12–16 respectively and invade the hippocampus by E14 (Tricoire et al. 2012).

A.2.2.1 Medial Ganglionic Eminence

In deeper analysis, The MGE gives rise to about 60% of LCNs in rodents. In terms of birthdate, MGE LCNs follow the same general inside-out relationship of birthdating to laminar location in the cortex as do the projection neurons. In addition to location and time, retroviral lineage analysis suggests that PV and SST interneurons can be derived from the same radial glial cell.

Within the MGE, the cascade begins with *Nkx2.1*, which acts as the master regulator in promoting MGE-derived interneuron fates. *Nkx2.1* is a gene with both activator and repressor function. Its repressor function attenuates the expression of CGE-specific genes, while its activator function induces the expression of the LIM homeodomain protein Lhx6. Lhx6 is expressed permanently in most MGE-derived LCNs from around the time of cell cycle exit (so

Lhx6+ interneurons are all post mitotic) and drives the expression of a series of factors including *Sox6* and *Satb1* whose actions selectively affect the development of both parvalbumin (PV)- and somatostatin (SST)-expressing interneurons. Lhx6 is expressed in the subventricular (SVZ) and submantle (MZ) zones of the mouse MGE from E11.5 to E17.5 and together with other transcription factors, secreted factors (e.g. reelin), chemorepellants and neurotransmitters (e.g. GABA) drive the interneurons to their final destination. All interneurons, unlike pyramidal neurons, migrate tangentially over long distances to populate the striatum, the cortex, the hippocampus and the amygdale (Figure 6A) (Kelsom and Lu 2013; Kepecs and Fishell 2014).

Expression of *Lhx6* is associated with GABAergic differentiation, whereas downregulation of *Lhx6* and combined expression of *Lhx7* and *Isl1* leads to cholinergic differentiation. *Lhx7* is also a LIM homeodomain protein that is induced in postmitotic cells in the SVZ and the MZ of the MGE, but unlike *Lhx6* is not expressed in tangentially migrating cortical interneurons but in ventral forebrain neurons that compose the cholinergic populations of the striatum and projection neurons of the basal forebrain (Figure 6B) (Fragkouli et al. 2009).

A.2.2.2 *Lhx6+* subclasses of interneurons

As shown in Figure 6A, *Lhx6+* interneurons can be subdivided to three non-overlapping populations:

1. PV+ interneurons express parvalbumin, a calcium binding protein which is involved in calcium signaling, and are consisted of two major types: soma-targeting basket cells that can be found in many brain regions, including the hippocampus, or chandelier cells targeting the axon initial segment that are located in the cortex. PVs control the timing of spikes with respect to theta oscillations in hippocampus. The dendritic domain of PV+ interneurons contains only a low density of voltage-gated Na+ channels and a high density of voltage-gated K+ channels. The high dendritic ratio of K+ to Na+ channels distinguishes PV+ interneurons from pyramidal cells and also from other interneuron subtypes. On the other hand, the axonal domain expresses an excessively high density of Na+ channels that contributes to rapid signaling in PV+ interneurons, so PV+ expressing interneurons are fast spiking. Hence, the excitability mechanism of PV+ cells is almost entirely axonal. Dysfunction of PV+ interneurons as far as their synaptic function, connectivity, timed transmission of information and regulation of gamma oscillations are concerned has been linked with epilepsy and schizophrenia (Hu, Gan, and Jonas 2014).

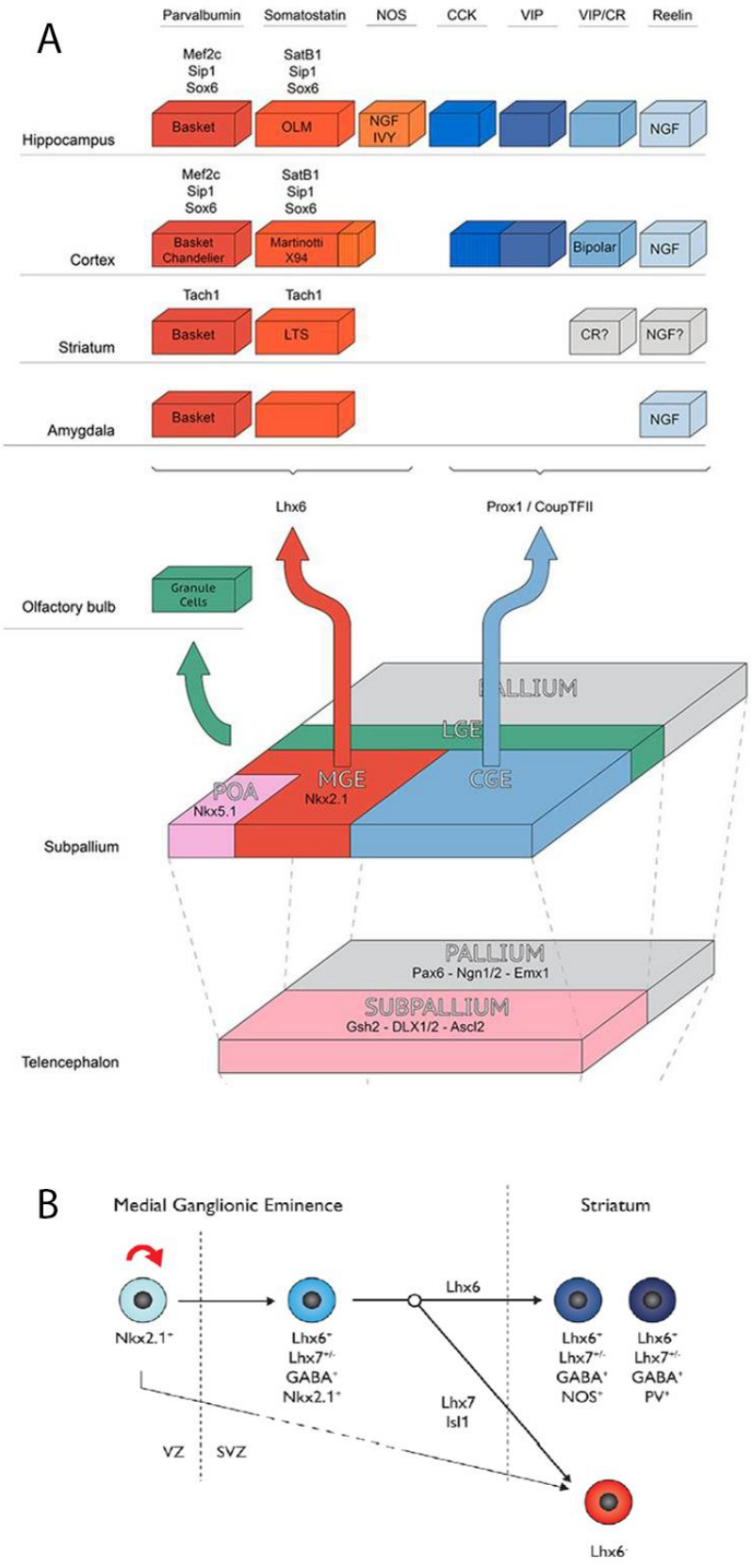

Figure 6. A) Fate of MGE-derived interneurons through Nkx2.1 and Lhx6 activation (adapted from Kepecs and Fishell, 2014) B) GABAergic differentiation of MGE-derived interneurons via Lhx6 regulation (adapted from Fragkouli et al, 2009).

2. SST+ interneurons express somatostatin, a growth hormone–inhibiting hormone (GHIH) that regulates the endocrine system and affects neurotransmission and cell proliferation, and are mainly cortical Martinotti neurons that locate the cortex and provide inhibition to the tufts of deep layer pyramidal cells. In hippocampus there are two low abundant subpopulations of OLMs and bistratified interneurons which inhibit the distal and proximal pyramidal dendrites respectively. They strongly suppress dendritic calcium spikes and bursting and can mediate di-synaptic inhibition between neighboring pyramidal cells. Dysfunctions in SST+ interneurons have been linked to kainate-induced, sensory-triggered seizures and cortex-mediated memory and learning deficits (Caroni 2015).

3. NOS+ interneurons express the neuronal nitric oxide synthase (nNOS), which is a family of enzymes catalyzing the production of nitric oxide (NO) from L-arginine, which is an important cellular signaling molecule, and compromise less than 1% of total hippocampal neurons and they have been linked with chronic mild stress and major depressive disorder (Marsden 2013).

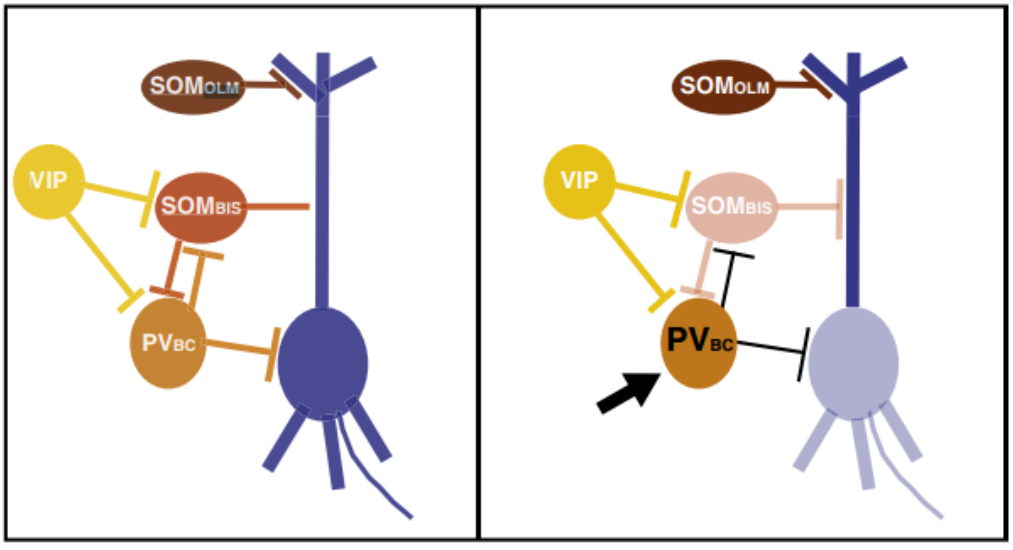

Figure 7. Left: Schematic presentation of local interneuron circuit in CA1 area of hippocmapus. Right: Excitation of PV BCs (black arrow) leads to disinhibition of the dendritic compartment (dark blue) but inhibition of the somatic compartment (pale blue) (adapted from Caroni, 2015)

A.2.3. Inhibitory plasticity – E/I balance

The plasticity of inhibitory neurotransmission has received relatively less attention than its excitatory counterpart despite its potential to deeply alter the function of neuronal networks. Inhibitory synapses, also known as symmetrical synapses (or type II) are non-uniformly distributed along the different subcellular compartments of pyramidal cells as shown before allowing selective integration of synaptic inputs in the soma and dendrites. The ability of inhibitory synapses to target specific subcellular compartments allows local control of clustered inputs (Flores and Mendez 2014). Inhibitory synapses have pre-synaptic vesicular GABA transporters (VGATs), which pack the inhibitory neurotransmitter GABA into synaptic vesicles for release, while the adaptor protein gephyrin help cluster y-aminobutyric acid receptors (ionotropic GABAARs and metabotropic GABABRs) and glycine receptors onto the postsynaptic surface (Gao and Penzes 2015).

Gephyrin is the main molecular organizer of inhibitory synapses and undergoes several post-translational modifications that affects clustering and interactions with major GABAA receptors, other regulatory proteins, siganlling complexes and cytoskeleton (Flores and Mendez 2014). In gephyrin KO animals, the loss of gephyrin from inhibitory synapses leads to death on postnatal day 0 (Feng et al. 1998). Collybistin is a regulator of the localization of gephyrin and an important determinant of inhibitory postsynaptic membrane formation and plasticity (Kins, Betz, and Kirsch 2000).

Synaptic activity driven functional changes of inhibitory neurotransmission are accompanied by modifications in the structure of GABAergic synapses with two major consequences: alteration of synaptic size and morphology and formation and elimination of inhibitory contacts (Figure 8). Maturation of GABAergic connectivity occurs both embryonically and during the first postnatal weeks, in an experience dependent manner. GABAergic inputs are initially depolarizing and become hyperpolarizing because of changes in chloride transporters, therefore, the organization of inhibitory synapses is thought to be carefully regulated over development and by experience to precisely match the organization, function, and strengths of excitatory synapses (Flores and Mendez 2014). The coregulation of excitation and inhibition is generally referred to as excitatory-inhibitory balance.

This ratio is highly asymmetric across development and between neuronal subtypes. For example, individual pyramidal cell dendrites in the cultured hippocampal cultures have E/I ratios of 2:1 at 14 days but 4:1 at 19 days (Liu 2004) while hippocampal parvalbumin and calretinin-positive interneuron subtypes have 14:1 and 3:1 ratios respectively (Gulyá et al. 1999). However, throughout life excitatory and inhibitory currents in a global scale tend to have a similar profile

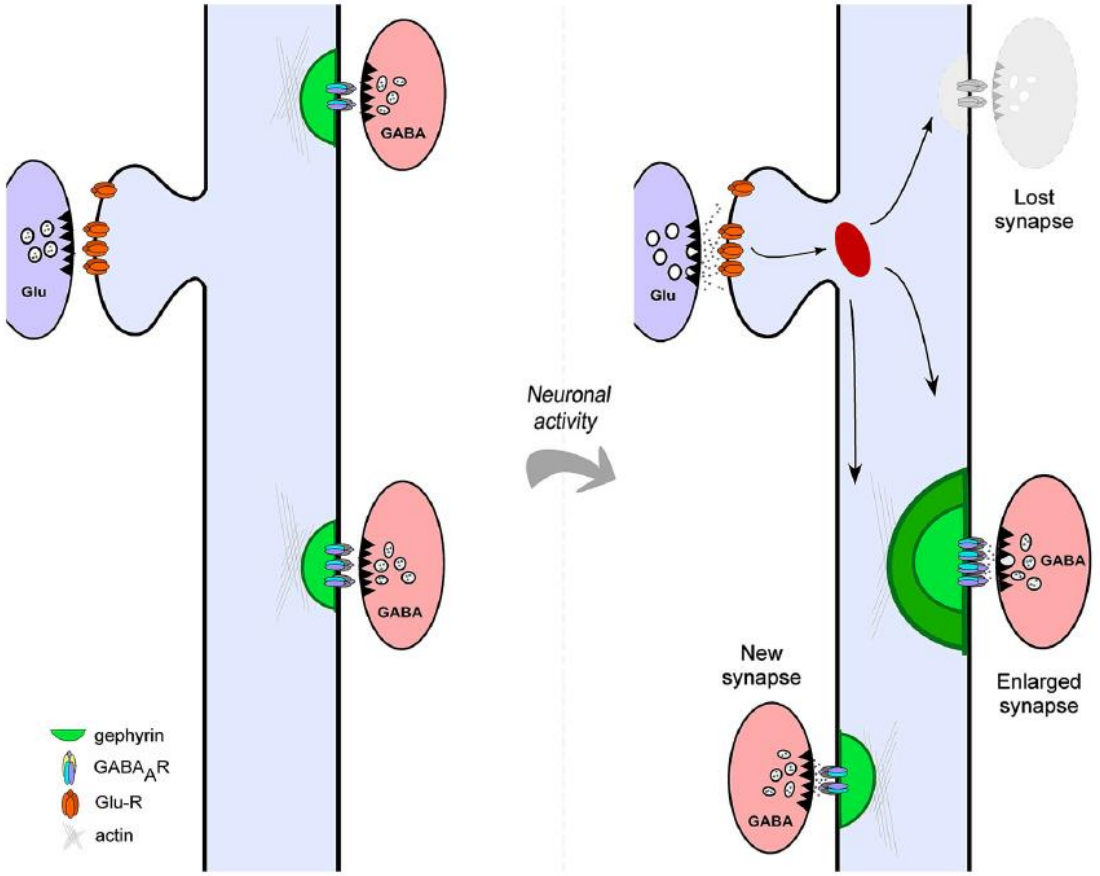

Figure 8. Structural plasticity of cortical GABAergic Synapses. Neuronal activity may alter the size of pre-existing inhibitory contacts or trigger complete elimination of GABAergic synapses (adapted from Flores and Mendez 2014).

in order to stabilize this ratio and maintain the neuronal activity in a safe range (Froemke 2015).

Imbalance of this ratio is linked with many diseases like autism (ASD), schizophrenia (SCZ) and epilepsy. Briefly, social and cognitive deficits that are present in both ASD and SCZ may arise from E/I imbalance because of dysfunctional initial neural circuit formation or maintenance. Also postmortem studies have discovered structural/functional changes in both

glutamatergic excitatory and GABAergic inhibitory circuits in individuals with ASD and SCZ (Gao and Penzes 2015). In addition, genetic deletion of *Tsc1* (Tuberous Sclerosis complex 1 that negatively regulated mTOR pathway) in the mouse hippocampus causes a cell-autonomous weakening of inhibitory input, which could result in increased seizure behavior and hyperexcitability at the network level (Bateup et al. 2013). Also mutation in phosphatidylinositol-3-kinase/phosphatase and tensin homolog (PTEN), another negative regulator of mTOR, produce epilepsy phenotypes and autistic-like deficits (LaSarge and Danzer 2014). mTOR pathway has also been linked with SCZ pathology, for example through AKT, essential for the PI3K-Akt-mTOR signaling cascade, as a candidate susceptibility gene related for SCZ, since its levels and kinase activity is significantly reduced in white blood cells and in postmortem brain tissue of schizophrenic patients (Gao and Penzes 2015).

However, the role of autophagy in shaping inhibitory synapses and thus dictating E/I balance has never been directly addressed.

B. Aim of the study

The aforementioned studies indicate the essential role of autophagy, as a major catabolic pathway serving for neuronal maintenance, in shaping the synapses in the central nervous system, and the importance of well-coordinated work between the different neuronal populations to properly maintain neuronal activity within a narrow, safe range.

The aim of this study is mainly, to investigate how autophagy shapes inhibitory synapses by generating a new mouse model where autophagy has been ablated in the MGE-derived interneurons and additionally, compare the deficits that mice demonstrate when autophagy has been ablated in inhibitory versus excitatory neuronal populations in different time periods.

C. Results

C.1. A model for ablation of autophagy in inhibitory neurons: Construction of mice with conditional ablation of *Atg5* in MGE-derived interneurons

Briefly, as mentioned in the introduction, brain inhibition is mainly facilitated by GABAergic interneurons. More than 60% of them are derived from the MGE, express the transcription factor Lhx6 when they exit their cell cycle and migrate tangentially to populate the striatum, the cortex, the hippocampus and the amygdale (Figure 9B). We generated conditional *Atg5* mutant mice (c*Atg5*KO) by crossing *Lhx6-cre* mice with mice carrying loxP-flanked (F) Atg5 alleles (Figure 9A).

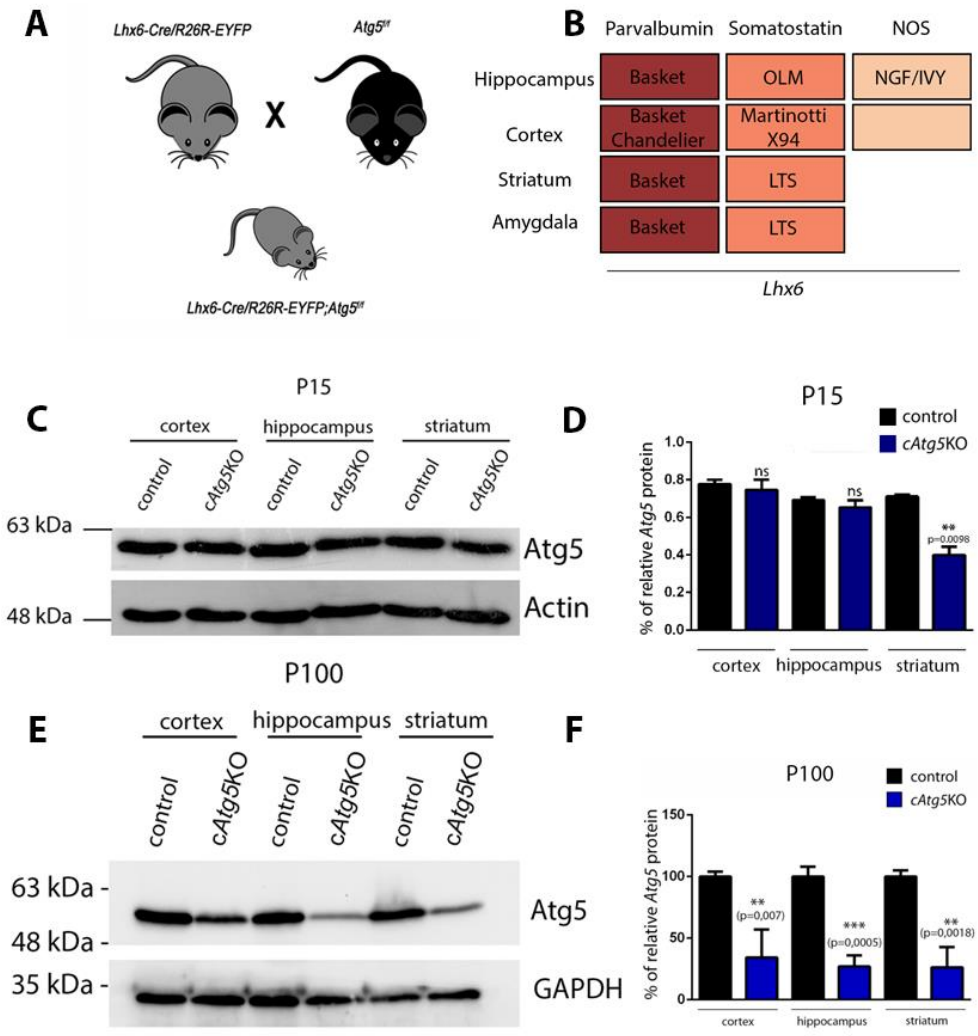

Figure 9. A) *Lhx6-Cre* mice, where Cre is expressed in MGE-derived interneurons, were crossed with *Atg5f/f* animals to obtain c*Atg5*KO mice. B) Subtypes of *Lhx6+* interneurons and the brain regions they migrate. C,E) Western blot with an antibody against Atg5 and D,F) Quantification of Atg5 protein levels in control (N=4) and c*Atg5*KO (N=4) brain areas, reveal the reduction of Atg5 in the cortex, hippocampus and striatum of c*Atg5*KO mice at postnatal days 15 and 100. Bars represent mean values ± SEM. Statistical analyses were performed using Student's t test.

The successful ablation of *Atg5* was confirmed biochemically by western blot analysis in two ages and three brain regions (Figure 9C,E). The reduction of Atg5 levels in the cortices and the hippocampi of pups (p15 group) shows no statistical significance since this population is estimated to consist only 10-15% of the total neuronal populations in these areas, unlike the striatum where the majority of *Lhx6+* interneurons are located (Figure 9D). As far as the adult animals (p100 group) the reduction of Atg5 levels is surprisingly more increased in all brain regions (Figure 9F), therefore we need to further investigate if there are apoptotic events or differences in the basal autophagic levels in inhibitory neurons of c*Atg5*KO animals.

C.2. *In vitro* primary neuronal cultures indicate increased cell body size and number of primary dendrites in c*Atg5*KO compared to control

We firstly sought to analyze *in vitro* the morphological effects that these autophagy-deficient interneurons display. To test this, we dissected embryos at embryonic day 16,5 and cultured primary cortical and striatal neurons for 7 days and observed increased cell body area (Figure 10A) and number of primary dendrites (Figure 10B) in c*Atg5*KO embryos compared to controls.

C.3. *In vivo* experiments demonstrating increased inhibitory markers, reduced spines and LTP deficits and in c*Atg5*KO animals

We next sought to determine if ablation of autophagy in MGE-derived interneurons increase inhibitory postsynaptic markers, so we performed assays for collybistin, a brain-specific GDP/GTP-exchange factor, and gephyrin, a scaffolding protein of inhibitory synapses. In parallel, we checked GAD65 levels, an enzyme that catalyzes the decarboxylation of glutamate

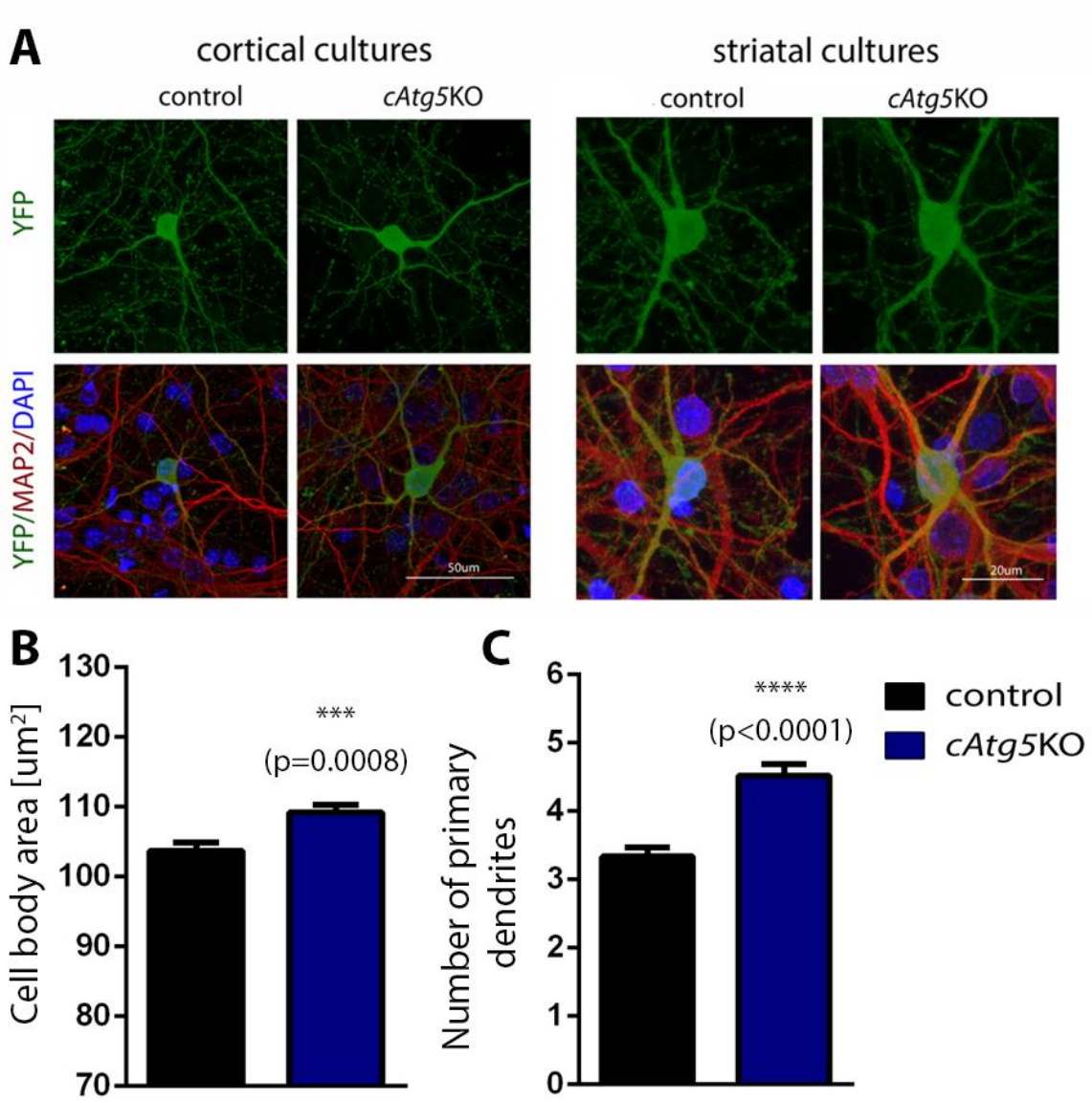

Figure 10. A) Confocal images of 7 DIV cortical and striatal neurons stained with an antibody against YFP, that stains *Lhx6+* interneurons, MAP2 and the nuclear dye Hoechst (DAPI). Graph showing quantifications with Operetta Software of the B) total cell body area and C) number of primary dendrites of Lhx6+ interneurons dissected and cultured from E16,5 c*Atg5*KO embryos (N=2 embryos, N=224 neurons) compared to controls (N=3 embryos, N=255 neurons). Primary cortical and striatal cultures at 7 DIV indicate increased cell body size and number of primary dendrites in c*Atg5*KO compared to controls. Bars represent mean values ± SEM. Statistical analyses were performed using Student's t test.

to GABA for neurotransmission and is a marker for all GABA-interneurons including the ones originating from MGE and express the *Lhx6* transcription factor (Figure 11A). Increased puncta, especially of gephyrin, but also of collybistin and GAD65 were observed in brain sections of stratum pyramidale (SP) of CA1 in a c*Atg5*KO animal compared to its littermate, which was also confirmed biochemically with western blot analysis (Figure 11B).

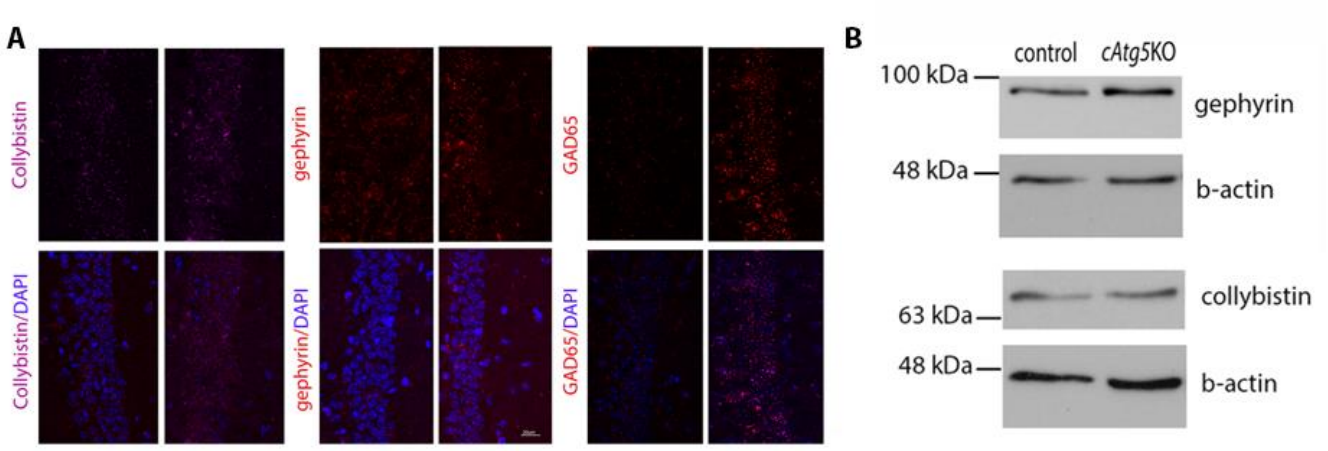

Figure 11. A) Immunohistochemistry in stratum pyramidale of CA1 demonstrates increased puncta of collybistin and gephyrin that mark inhibitory postsynaptic densities and increased levels of presynaptic GAD65 in a c*Atg5*KO animal compared to its control. B) Western blot analysis for gephyrin and collybistin in cortical lysates of adult control and c*Atg5*KO animals.

In addition, we focused on the structural effects that these autophagy-deficient interneurons may cause *in vivo* in their targeted pyramidal neurons. Notably, we found that adult c*Atg5*KO animals exhibit significantly decreased number of dendritic spines on CA1 pyramidal neurons compared to controls (Figure 12B), whereas c*Atg5*KO pups do not (Figure 12A). This reduction is present in all type of dendritic spines (thin-stubby, mushroom, filopodia) as revealed by Golgi-Cox staining.

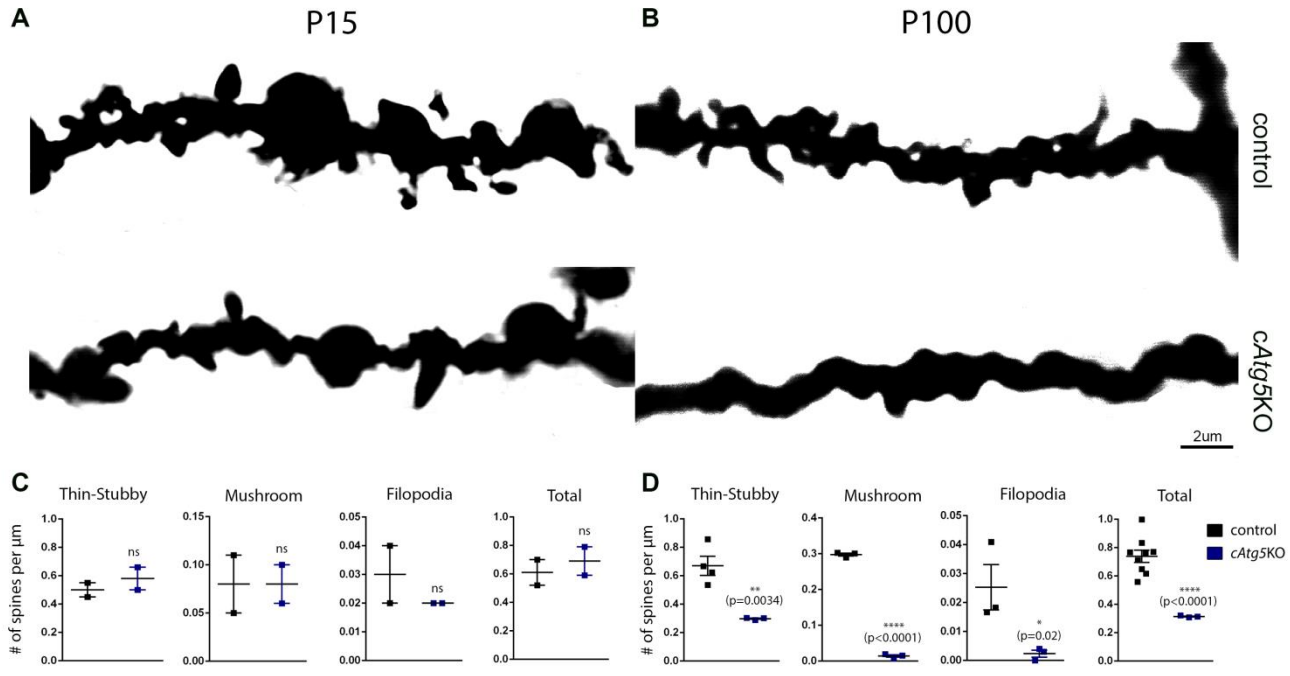

Figure 12. A-B) Brightfield photomicrographs illustrating Golgi-impregnated distal dendrites and spines on CA1 pyramidal neurons from c*Atg5*KO mice (blue, N=1 & N=3 at p15 and p100 groups respectively) and control littermates (black, N=1 & N=4 at p15 and p100 groups respectively) at postnatal days 15 and 100. C-D) Graphs showing quantification of all types of spines at postnatal days 15 and 100. Note that C) adult mice (p100) c*Atg5*KO mice demonstrate reduced thin-stubby, mushroom-like and filopodia types of spines, whereas D) pups (p15) do not. Scatter plots represent mean values ± SEM. Statistical analyses were performed using Student's t test.

We then sought to determine whether ablation of autophagy in MGE-derived interneurons can cause LTP defects (Figure 13). As expected, c*Atg5*KO animals (blue, N=3 animals and N=14 slices) exhibit an LTP-deficit in CA3-CA1 synapses compared to their control littermates (black, N=5 animals and N=14 slides).

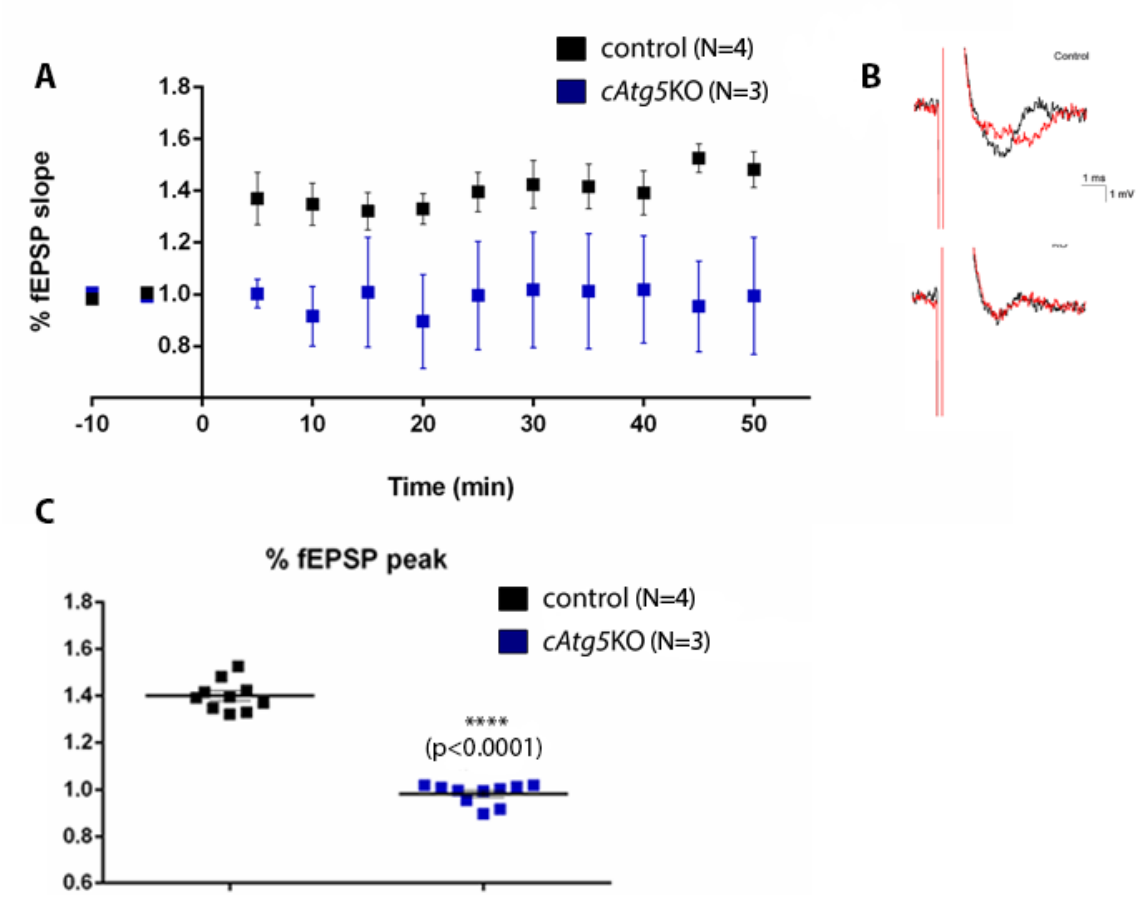

Figure 13. A) Percentage of fEPSP slope before and after theta burst stimulation. B) Representative traces of a pre-theta burst (black) voltage response and a post-theta burst (red) voltage response. C) Normalized slope of fEPSP for 15 min following theta-burst stimulation of the CA3-CA1 synapses. Note that the c*Atg5*KO exhibits an LTP-deficit. Scatter plot represents mean values ± SEM. Statistical analyses were performed using Student's t test.

C.4. Behavioral characterization of c*Atg5*KO animals demonstrating memory deficits, resistance to seizures and general anxious-like behavior

Next, we were curious if these animals demonstrate altered memory formation. Notably, we found that c*Atg5*KO (N=9) animals exhibit significantly decreased freezing (Figure 14A) in a contextual fear conditioning test compared to controls (N=9), indicating that they have

decreased fear memory formation, since they do not demonstrate any different response to the new environment or the delivered shock (Figure 14B-C).

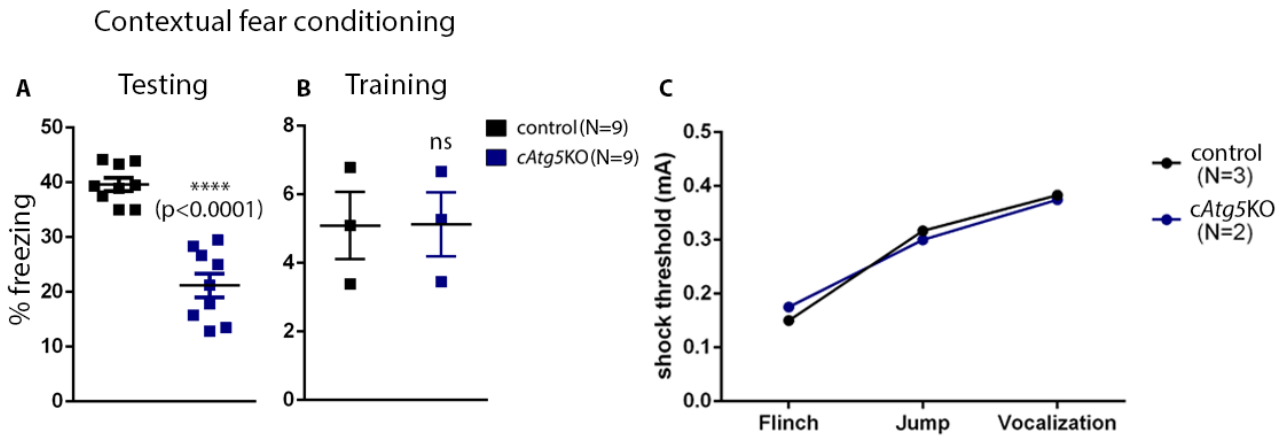

Figure 14. A) *Lhx6* autophagy deficient mice demonstrate decreased freezing response in a contextual fear conditioning test, but no difference in B) freezing during the training day or the C) mean current threshold intensity (mA) according to flinch, jump and vocalization responses (Error bars were not included because they overlapped at all points). Scatter plots represent mean values ± SEM. Statistical analyses were performed using Student's t test.

We then sought to further behaviorally characterize these animals, so we performed three anxiety-related behavioral tasks (Open Field Test, Elevated Plus Maze, Light-Dark box Test) and measured their preference for the compartments of the devices that mice generally feel more vulnerable to environmental dangers and tend to avoid (Figure 15A-C). In all three anxiety-related tasks c*Atg5*KO mice spent less time in these "more exposed" compartments, indicating that they exhibit anxious-like behavior compared to their control littermates. In addition, c*Atg5*KO animals were tested for their resistance to seizure behavior after injecting with pilocarpine, demonstrating lower mortality rate than their control littermates (Figure 15D).

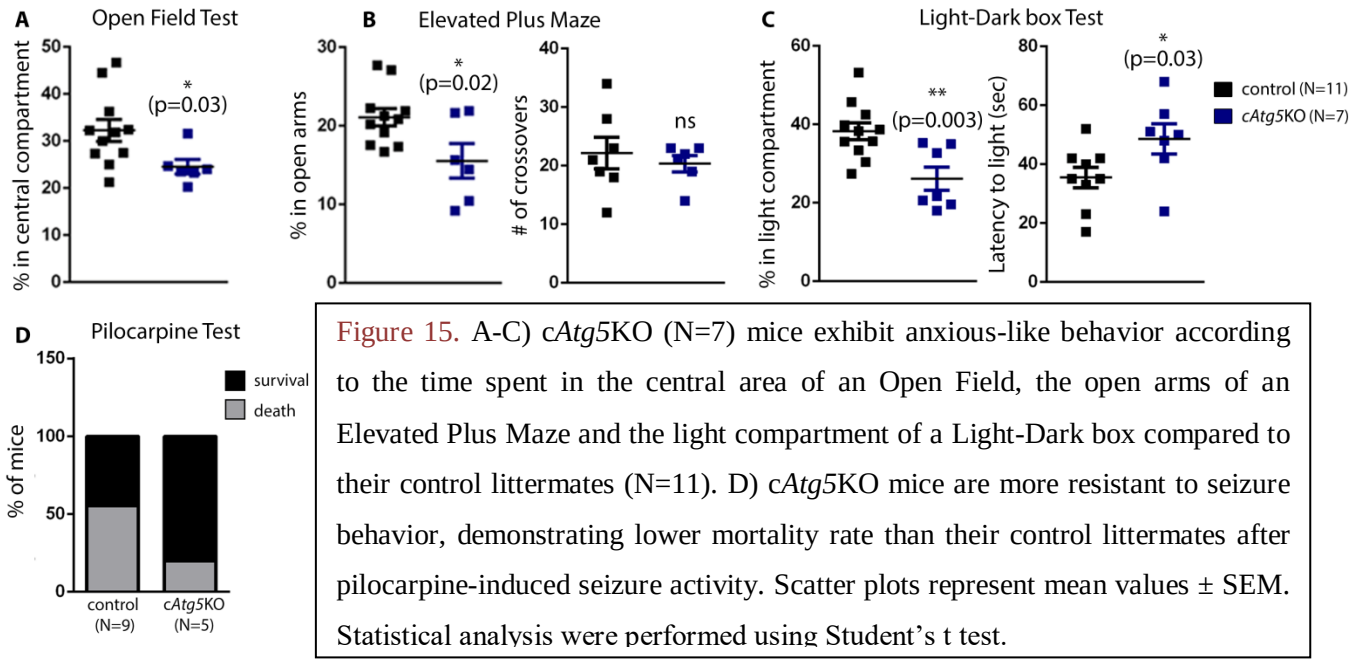

Figure 15. A-C) c*Atg5*KO (N=7) mice exhibit anxious-like behavior according to the time spent in the central area of an Open Field, the open arms of an Elevated Plus Maze and the light compartment of a Light-Dark box compared to their control littermates (N=11). D) c*Atg5*KO mice are more resistant to seizure behavior, demonstrating lower mortality rate than their control littermates after pilocarpine-induced seizure activity. Scatter plots represent mean values ± SEM. Statistical analysis were performed using Student's t test.

C.5. Construction of a new mouse model that *Atg5* is ablated in the majority of pyramidal neurons in different time periods (p15-pups or p60-adult)

In parallel, we generated conditional *Atg5* mutant mice (*Thy1*-c*Atg5*KO) by crossing *Thy1-cre* mice with mice carrying loxP-flanked (F) Atg5 alleles. This ablation is inducible, so allows us to control gene activity at specific time points after injecting the mice intraperitoneally with tamoxifen. The reduction of Atg5 levels were confirmed in cortices of animals that were injected at postnatal day 45 (Figure 17A).

As far as the p15 group is concerned, our model verifies the decrease in pruning of pre-existing spines that was proposed by another model where autophagy is conditionally ablated in similar time periods in *CamkII*+ pyramidal neurons (Tang et al. 2014) by the failure of *Thy1-Atg5*KO animals to induce Long Term Depression (Figure 16A-B), whereas they exhibit no anxiety-like behavior (interestingly slight significant difference exists only in the time spent in open arms of an Elevated Plus Maze) (Figure 16C-E).

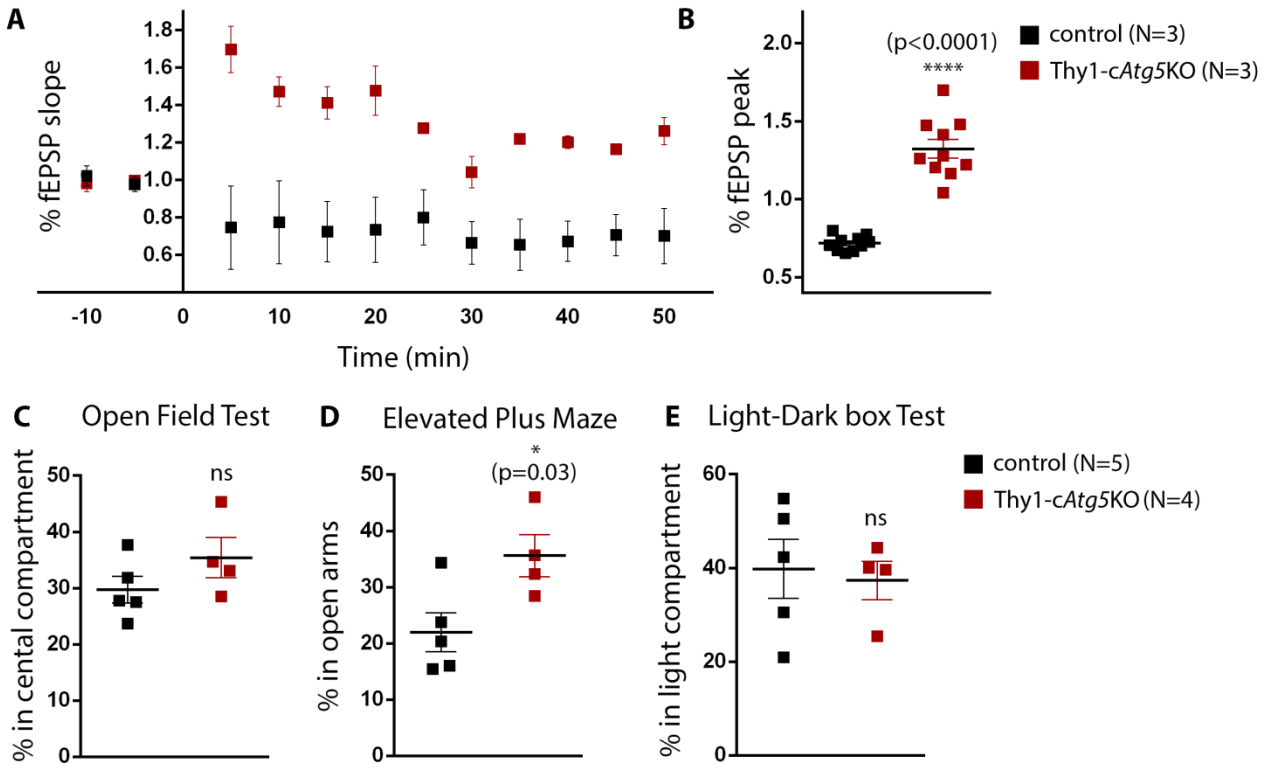

Figure 16. A) Percentage of fEPSP slope before and after Low Frequent Stimulation (LFS). B) Normalized slope of fEPSP for 15 min following LFS. Note that the p15 injected *Thy1-Atg5*KO (N=3 animals and N=9 slices) cannot induce Long Term Depression compared to their controls (N=2 animals and N=7 slices).C-E) p15 injected *Thy1-Atg5*KO (N=4) mice do not exhibit (or slightly less as far as the EPM is concerned) anxious-like behavior according to the time spent in the central area of an Open Field, the open arms of an Elevated Plus Maze and the light compartment of a Light-Dark box compared to their control littermates (N=5). Scatter plots represent mean values ± SEM. Statistical analyses were performed using Student's t test.

On the other hand, autophagy deficient animals in pyramidal neurons during adulthood (p60 group) demonstrate no LTP-deficits, no hippocampus-dependent memory defects and no anxiety-like behavior (Figure 17B-G).

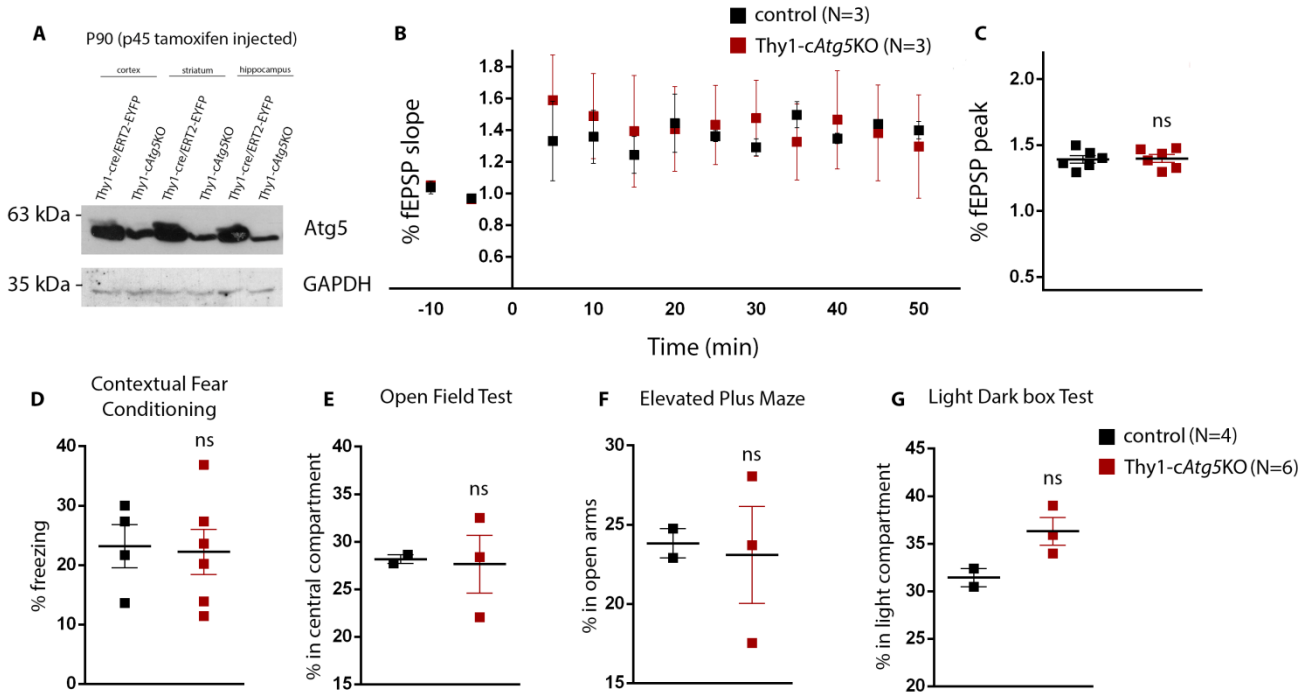

Figure 17. A) Western blot with an antibody against Atg5 in three different regions in an adult *Thy1-Atg5*KO animal compared to a *Thy1-cre/ERT2-EYFP* animal, both injected with tamoxifen at p45 day. B) Percentage of fEPSP slope before and after theta burst stimulation C) Normalized slope of fEPSP for 15 min following theta-burst stimulation of the CA3-CA1 synapses. Note that the p60 injected Thy1-*Atg5*KO (N=3 animals and N=10 slices) do not exhibit an LTP-deficit compared to their controls (N=3 animals and N=9 slices). D) p60 injected *Thy1-Atg5*KO mice (N=6) demonstrate equal freezing response with their control littermates (N=4) in a contextual fear conditioning test. E-G) p60 injected *Thy1-Atg5*KO (N=6) mice do not exhibit anxious-like behavior according to the time spent in the central area of an Open Field, the open arms of an Elevated Plus Maze and the light compartment of a Light-Dark box compared to their control littermates (N=4). Scatter plots represent mean values ± SEM. Statistical analyses were performed using Student's t test.

D. Discussion

D.1. Does autophagy deficiency in interneurons result in increased brain inhibition?

Our results indicate that ablation of autophagy even in a small neuronal population in the brain can result in a variety of defects in the mice, but the mechanism by which autophagy-deficient interneurons cause these non cell autonomous effects still remains unknown. One emerging hypothesis is that brain inhibition is increased, consequently the E/I ratio is decreased. In order to verify this hypothesis, patch clump recordings need to be performed and give us important information not only for the inhibitory current status of the autophagy-deficient interneurons but also the excitatory current status of the pyramidal neurons in the same area.

The hypothesis that brain inhibition is increased was firstly created because of the increased number of primary dendrites from the *in vitro* analysis, which makes possible that *Lhx6-Atg5*KO animals contain more functional inhibitory synapses inside the neuronal network. However, we are not sure of the mature state of the interneurons in the cell cultures and if autophagy is implicated in GABA switch, the process that GABA has no longer excitatory but inhibitory action (Figure 18A). The proper timing of GABA transition from depolarizing to hyperpolarizing is fundamental for a correct development of the brain. The timing of this switch is controlled by upregulating activity of the chloride co-transporter KCC2 (Leonzino et al. 2016) which is known to be down-regulated by rapamycin treatment, the main inhibitor of the mTOR pathway (Huang et al. 2012), and up-regulated by BDNF, the master regulator of autophagy, in epileptic hippocampi (Eftekhari et al. 2014). Even though autophagy has never been directly linked with the GABA switch, it is important to use mature GABA+ interneurons for our study, so the duration of cell cultures should be expanded to 15 or 21 days. Also, apart from staining the whole autophagy-deficient interneuron, it is of high demand to molecularly detect the functional inhibitory synapses by staining not only the postsynaptic density with the already used gephyrin but also the presynaptic area with a marker for inhibitory presynaptic buttons like synaptophysin2, a component of the synaptic vesicle membrane that plays essential role in synaptic vesicle trafficking.

As far as the *in vivo* approach is concerned, golgi staining revealed a decrease in the number of dendritic spines in adult animals (p100) but no difference in pups (p15). Between

these two time points, pruning period, when excess dendritic spines are eliminated, is the most critical period for stabilization of the neuronal networks, so we need to further investigate if this overmuch elimination of dendritic spines takes place during pruning period or not. For this reason, golgi stainings should be also performed in p30-p35 mice, where dendritic pruning has just been completed.

To gain mechanistic insight, we need to investigate how the proposed increased inhibition in the network level leads to structural changes in the pyramidal neurons. Increased inhibition is translated into increased release of GABA neurotransmitter in the synaptic cleft. But what does excessive GABA cause in the dendrites of the pyramidal neurons? It was found that when GABAergic inputs are followed shortly by action potentials in a well established LTD protocol (Figure 18B), spine shrinkage was reliably induced (Figure 18D) when back-propagating action potentials were paired with GABA uncaging at the dendritic shaft close to the stimulated spine in less than 5μm from the input point (Figure 18C). This shrinkage was $GABA_A$ receptor mediated, since it was present after muscimol treatment (an agonist of $GABA_A$ receptors) and abolished when antagonists of NMDA receptors (APV, MK-801) were applied. It was suggested that $GABA_A$ receptors promoted spine shrinkage by suppressing back-propagating action potentials that trigger bulk increases in intracellular concentration of calcium $[Ca^{2+}]i$. Reduction in bulk increases in global $[Ca^{2+}]i$ was able to replace the effects of GABA, as the cytosolic application of EGTA (a chelating agent with high affinity for calcium ions) mimicked the effects of GABA. Thus, $GABA_A$ receptors themselves were not required for spine shrinkage, as long as $[Ca^{2+}]i$ increases were in the appropriate range. The $[Ca^{2+}]i$ increase had to be high enough to prohibit spine shrinkage and the $[Ca^{2+}]i$ increase needed to be suppressed by GABAergic inhibition or EGTA to induce spine shrinkage (Hayama et al. 2013). To conclude, the excitation-inhibition balance affects synaptic contacts not only by the modulation of spike activities but also more directly by the GABAergic inhibition of local dendritic Ca^{2+} signaling.

Going back to our model with the proposed increased inhibition, inhibition of local dendritic Ca^{2+} signaling would cause elimination of dendritic spines at adult mice that will alter the synaptic plasticity of the brain and general the behavior of the mice. Behavioral characterization of *Lhx6-Atg5*KO mice should be continued in order to create a general

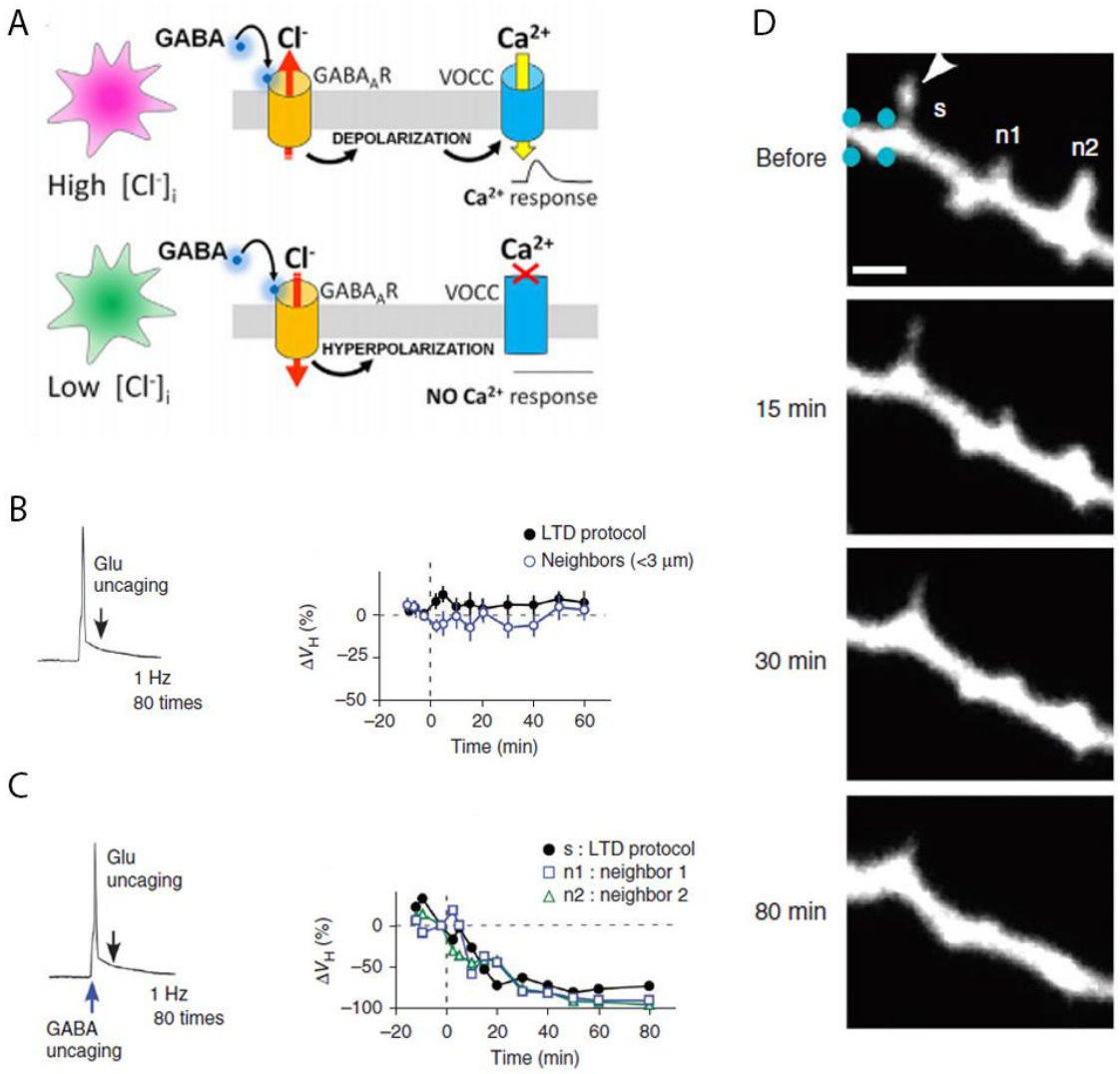

Figure 18. A) GABA neurotransmitter has no longer excitatory but inhibitory action B) spine shrinkage is not induced when back-propagating action potentials (bAPs) preceded glutamate uncaging but C) when each bAP was paired with GABA uncaging D) Spine shrinkage tended to spread to neighboring spines for a distance of up to approximately 15 µm (Scale bar: 2 µm) (adapted from (Hayama et al. 2013)

behavioral profile of these animals. Briefly, social interaction (choose between a familiar and a novel mouse) or social recognition memory tests (explore a novel social partner) that demonstrate a defective social phenotype in animals that autophagy has been ablated in other population, like pyramidal neurons or microglia should be also conducted to *Lhx6-Atg5*KO

animals. In addition, depression has been linked with defective mTOR-dependent synaptic plasticity (Marsden 2013), so Force Swimming Test (FST), the most accurate depression test where mice are placed in an inescapable transparent tank that is filled with water and try to escape should give a hint for the possible role of autophagy in this type of disease. Finally, other memory tests and not exclusively hippocampal-dependent, like Morris Water Maze where the mouse has to find its way to a hidden platform in a pool full of water only with the help of surrounding cues and landmarks, should also be performed to specialize the memory deficits these *Lhx6-Atg5*KO animals exhibit.

D.2. Generation of double-cre autophagy deficient mice

As mentioned before, it is well known that mice where autophagy has been ablated in the forebrain excitatory neurons demonstrate neuronal hyperexcitability and LTD-like deficits that resemble epileptic and autistic behavior. However, in this mouse model (*CamkII-cre;Atg7*$^{f/f}$) autophagy has been ablated in a fixed time point, during the pruning period. Since our results suggest that autophagy may be critical for specific time periods, we will take advantage of the inducible *Thy1-cre;Atg5*$^{f/f}$ mouse model and try characterize the temporal activity of autophagy in the neuronal networks and its contribution to subsequent severe autistic or/and epileptic phenotype. In addition, we will cross *Thy1-cre;Atg5*$^{f/f}$ and *Lhx6-cre;Atg5*$^{f/f}$ mice to obtain double-cre *Thy1-cre;Lhx6-cre; Atg5*$^{f/f}$ animals and question ourselves if the defects demonstrated at the p15 or p60 injected *Thy1-cre;Atg5*$^{f/f}$ animals, can be rescued in these double-cre animals.

Taken together, these experiments will give us novel insight, firstly, on the role of autophagy in synaptic function at different time periods and, secondly, on the 'opposing' role of ablation of autophagy in excitatory versus inhibitory neuronal subpopulations

E. Materials and Methods

E.1. Mice

All mice were housed with ad libitum access for food and water, and maintained with constant temperature and humidity in a 12 hr/12 hr light/dark cycle. All experiments were

performed in accordance with the guidelines of FORTH ethics committee. All animals used were mice of C57BL/6 genetic background.

Lhx6-Cre/R26R-EYFP (Lim homeobox 6, Lhx6)–Cre transgenic mice (a generous gift of Dr. Karagogeos – Medical Department of University of Crete) express Cre recombinase and Enhanced Yellow Fluorescent Protein in the migratory interneurons derived from the Medial Ganglionic Eminence, as previously described (Fogarty et al. 2007).

B6.Cg-Tg(Thy1-cre/ERT2,-EYFP)HGfng/PyngJ (*THYmocyte differentiation antigen 1, Thy1)-Cre* mice were generated by Jackson laboratory and express a tamoxifen inducible Cre-mediated recombination system and Enhanced Yellow Fluorescent Protein in the majority of projection neurons populations in the central and peripheral nervous system. Tamoxifen (Sigma-Aldrich) was dissolved in corn oil (20mg/ml) at 37^{o}C and administered intraperitoneally for 5 consecutive days at male mice (75mg/kg), as recommended by Jackson laboratory (https://www.jax.org/research-and-faculty/resources/cre-repository/tamoxifen). Mice were left undisturbed for at least 7 days before any experimental procedure.

Atg5flox/flox mice (a generous gift of Dr. Chamilos- Medical Department of University of Crete) were crossed with *Lhx6-cre* and *Thy1-cre* mice to generate animals where *Atg5* is conditionally ablated in inhibitory and excitatory populations respectively.

E.2. Genotyping

Mouse genomic DNA was isolated from tail biopsies following 1h incubation at 95^{o}C in 60ul Denaturating Buffer (25mM NaOH, 0,2mM EDTA) and equivalent neutralization (40mM Tris pH=8). The primers below were used to detect the existence of *Lhx6-cre*, *YFP*, *Thy1-cre* and the *Atg5* flox allele.

Lhx6-cre 250 F	5'-GAGGGACTACCTCCTGTATC-3'
Lhx6-cre 880 R	5'-TGCCCAGAGTCATCCTTGGC-3'
MEH F	5-AAGTGAGTTTGCATGGCGCAGC-3'

MEH R	5’-CCCTTTAGCCCCTTCCCTCTG-3’
YFP LC	5’-GCTCTGAGTTGTTATCAGTAAGG-3’
YFP R2	5’-GCGAAGAGTTTGTCCTCAACC-3’
YFP R3	5’-GGAGCGGGAGAAATGGATATG-3’
Thy1-oIMR7303-F	5’-TCTGAGTGGCAAAGGACCTTAGG-3’
Thy1-oIMR8744-F-PC	5’- CAAATGTTGCTTGTCTGGTG-3’
Thy1-oIMR8745-R	5’-GTCAGTCGAGTGCACAGTTT-3’
Thy1-oIMR9296-R-PC	5’-CGCTGAACTTGTGGCCGTTTACG-3
Atg5-1	5’-ATATGAAGGCACACCCCTGAA-3’
Atg5-2	AACGTCGAGCACAGCTGCGCAA-3’
Atg5-3	5’-ACTGCATAATGGTTTAACTCTT-3’

E.3. Western Blotting

Tissues were lysed in RIPA buffer (500 mM Tris-HCl pH 7.2, 1MNaCl, EDTA, Triton 100-X, Na-deoxycholate, 10% SDS), containing protease inhibitors (Roche) and sonicated for 2x15 seconds on ice. They were incubated overnight on ice and centrifuged at 13,200 rpm for 30 minutes. Bradford method was used to measure the concentration of the samples, which then were separated on a 7,5-12% polyacrylamide gel and transferred to a nitrocellulose membrane. After blocking for 1 hour at room temperature in 5% skim milk, membranes were incubated in

the primary antibodies overnight at 4ºC. After washing (3x10 minutes) in TPBS (100 mM Na2HPO4, 100mM NaH2PO4, 0.5N NaCl, 0.1% Tween-20), membranes were incubated for 1 hour at room temperature in corresponding secondary horseradish peroxidase-conjugated antibodies in 2% milk solution in TPBS. Blots were washed (3x10 minutes) and developed by chemiluminescence (Supersignal chemiluminescent substrate, pico and fempto, Thermo Fisher Scientific) according to the manufacturer's instructions.

The primary antibodies used were atg5 (Abcam), gephyrin (Synaptic Systems), collybistin (Synaptic Systems), GAPDH (Santa Cruz) and b-actin (Santa Cruz). The secondary antibodies used were horseradish peroxidase-conjugated anti-mouse and anti-rabbit (Abcam, both 1:10000).

E.4. Immunohistochemistry - Immunofluorescence

Mice were anaesthetized with 2,5% avertin (16ul/g) and then perfused with 4% paraformaldehyde in PBS buffer. Brains were further post-fixed for 2-4 hours before storing in 30% sucrose in PBS at 4ºC. After 2-3 days, when the brains were submerged, they were quickly frozen in OCT and stored in -80ºC. Coronal or sagittal slices of 18um were cut in Leica CM1950 cryostat and slides were heated at 37ºC for 1-2 hours before storage in -80ºC.

Tissue sections were re-hydrated with PBS (15 minutes) and incubated for 1h in blocking solution (10% fetal bovine serum and 0.2% Triton-X in PBS) at room temperature and overnight with primary antibodies in blocking solution at 4ºC. The sections were rinsed with PBS (3 washes x 10 minutes) and incubated with secondary antibodies in PBS for 1 hour at dark. Finally, the sections were rinsed again in PBS (4 washes x 10 minutes), dipped 2 times in distilled water and mounted with 80% glycerol. The primary antibodies used were collybistin (Synaptic Systems), gephyrin (Synaptic Systems) and GAD65. The secondary antibodies used were anti-rabbit conjugated to Alexa Fluor 488, anti-mouse conjugated to Alexa Fluor 594 and Hoechst 33342 (1:5000) which dyes the nucleus.

E.5. Neuronal cultures

In order to specify the embryonic day, the time of plug was counted as day 0.5. The cortices and striata of embryonic day 16.5 (E16.5) per embryo were dissected in PBS. After

washing and centrifugation (2 x 5 minutes at 1000 rpm), cells were treated with 0.25% trypsin at 37^{o}C followed by mechanically dissociation. After inactivation of the trypsin with DMEM/FBS solution, cells were plated in 24-well plates containing 13-mm glass coverslips, coated overnight with poly-D-lysine (Sigma-Aldrich), and cultured in Neurobasal medium (GIBCO) supplemented with B-27 (2%), L-glutamine (300 mM), penicillin (5 mg/ml), and streptomycin (12.5 mg/ml) and 25uM b-mercaptoethanol. The initial density was 250.000 cells/cm2 in a final volume of 1 ml/well. At 7 days in vitro (7 DIV), neurons were fixed for 20 minutes with 4% paraformaldehyde at room temperature, rinsed and stored in PBS at 4^{o}C.

E.6. Immunostaining

Cells were incubated for 1 hr in blocking solution (10% fetal bovine serum and 0.2% Triton-X in PBS) at room temperature and overnight with primary antibodies in blocking solution at 4^{o}C. The following primary antibodies were used: GFP and MAP2 (Synaptic System). Neurons were rinsed in PBS (3 x 10 minutes) and incubated with the following secondary antibodies for 1 hour at room temperature and dark: anti-rabbit Alexa 488, anti-guinea pig Alexa 647 and Hoechst 33342 (1:5000). Neurons were rinsed in PBS (4x10 minutes), dipped in distilled water and mounted onto slides. Confocal images of fluorescently labeled proteins were captured using the LSM 710 NL multi-photon microscope (Zeiss). The cell body area and the number of primary dendrites were measured with Operetta Software that scans the whole coverslip and identifies neurons as mass fluorescent pixels.

E.7. Golgi staining

Brains of mice at postnatal days 15 or 100 (at least 1 week after any behavioral experiment) were removed and placed in Golgi-Cox solution (5% Potassium Dichromate, 5% Mercuric Chloride (sublimate) and 5% Solution of Potassium Chromate), which had been prepared at least 5 days earlier. Brains remained in Golgi-Cox solution for 14 days at room temperature at dark refreshing the medium every 2-3 days, then submerged in 30% sucrose solution at 4^{o}C and subsequently sliced (150 mm thick slices) in a vibratome (Leica VT 1200S) in 6% sucrose bath. The slices were placed onto superfrost microscope slides, covered with parafilm, and maintained in a humidity chamber for 2-3 days. The parafilm was then removed, and the slides were incubated first in ammonium hydroxide for 15 min and then in Kodak Fix

solution in a dark room for 15 min followed by washes with PBS (1minute). The brain slices were then dehydrated with increasing concentrations of ethanol (50% - 1min, 70% - 1min, 95% - 1min, and 100% - 3min) incubated in xylene for 4 min and coverslipped with 80% glycerol. The slides were kept for at least 45 days before imaging under the 63X lens of a confocal microscope (LSM 710 NL multi-photon microscope-Zeiss). Proximal and distal dendritic segments from pyramidal neurons in the CA1 area from each animal were analyzed for the number of all types of dendritic spines.

E.8. Anxiety-related tests

Male mice at postnatal days 32-35 were tested for three different anxiety-related behavioral tests at three consecutive days. Mice were bred at the animal facility of FORTH and transferred to the Department of Biology (Sidiropoulou's animal house) at least 5 days before any experiment in order to adapt to the new facility. Mice were isolated from their brothers and habituated to the experimental room for 1 hour.

E.8.1. Open Field Test

Mice (one at a time) were placed in the center of a 50x50x50 cm open field device and left undisturbed to freely explore the device for 15 minutes. The time spent in the central compartment was calculated.

E.8.2. Elevated Plus Maze

Mice (one at a time) were placed in the center of a 70x70x45 elevated plus maze facing a closed arm and left undisturbed to freely explore the device for 5 minutes. The time spent in the open arms and the total number of crossovers between the arms were calculated.

E.8.3. Light-Dark Box Test

Mice (one at a time) were placed in the dark compartment of a 60x30x30 (40% light compartment) box. An obstacle blocking the intermediate door between the two compartments was removed after 10 seconds and mice were free to explore the device for 5 minutes. The time spent in the light compartment and the latency to firstly enter the light compartment were calculated.

During these three anxiety-related tests the experimenter was outside of the room to reduce as much as possible the stress produced by the human presence. After the last experiment brother mice were united again till the next one.

E.9.1 Contextual Fear Conditioning

The same mice were tested at Contextual Fear Conditioning test when they reached two and a half months. They were isolated again from their brothers and habituated to the experimental room for 1 hour. Mice (one at a time) were placed in the fear conditioning chamber (MedAssociates), which was controlled through a custom-made interface connected to a computer. After 7min of habituation to the conditioning chamber, each mouse received one strong foot-shock (1000ms, 0.75 mA), and remained in the chamber for another 3min. The next day mice were returned to the training chamber with exactly the same contextual information (e.g. odor, light, temperature, visual cues) without providing any shock for 9 minutes. The percentages of freezing behavior during the first three minutes of the training day and the full duration of the testing day were measured.

E.9.2. Test shock response

Different groups of mice were tested for their response to foot shock. Mice were placed in the fear conditioning chamber, and 4 minutes later they received a train of 0.75-s shocks spaced 30 seconds apart. The mouse was scored as to whether it flinched, jumped, or vocalized to the shock, as previously described (J. J. Kim et al. 1991). Flinch was a temporarily immobilization and an orienting response of the head usually directed at the grid floor. Jump was any jumping or running response to the shock. Vocalization was any audible response to the shock. The shock intensity of the train of shocks had the following progression: 0.15, 0.25, 0.35, 0.45, 0.55 and 0.65 mA. As soon as all three responses were scored in two consecutive series, the series ended. (Shocks greater than 0.65 mA were never needed.) In this manner, three current values were obtained for each response.

E.10. Pilocarpine model

Male mice, 2 months old were tested for seizure behavior, which was induced by intraperitoneal administration of 250mg/kg pilocarpine (Sigma-Aldrich). Animals were recorded

for 2 hours during the seizure period to determine the duration and severity of seizure activity on a 0–7 rating scale as previously described (Morrison et al. 1996)

All behavioral experiments were blind tests to the genotype of the mice and all the measurements were analyzed manually using J-Watcher software (http://www.jwatcher.ucla.edu/).

E.11. Electrophysiology

Electrophysiological experiments were performed, at least one week after any behavioral experiment, using in vitro slice preparation. The brain was removed immediately after decapitation and placed in ice cold, oxygenated (95% O_2/5% CO_2) artificial cerebrospinal fluid aCSF (namely 0 Ca^{2+} aCSF, 125mM NaCl, 3,5mM KCl, 26mM $NaHCO_3$, 1,26mM NaH_2PO_4, 3 $MgCl_2$, 10 mM glucose and pH = 7,4). The brain part containing the hippocampus was blocked and glued onto the stage of a vibratome (Leica, VT1000S, Leica Biosystems GmbH, Wetzlar, Germany). 400 μm thick brain slices containing the hippocampus were taken and transferred to a submerged chamber, which was continuously superfused with oxygenated (95% O_2/5% CO_2) aCSF (namely control aCSF, 125mM NaCl, 3,5mM KCl, 26mM $NaHCO_3$, 2mM $CaCl_2$, 1mM $MgCl_2$, 10mM glucose and pH=7,4) at room temperature. Extracellular recording electrodes filled with NaCl (3M) were placed in the *stratum radiatum* (SR) layer of the CA1 region. Platinum/iridium metal microelectrodes (Harvard apparatus UK, Cambridge, UK) were also placed in the SR layer, about 300 μm away from the recording electrode, and were used to evoke fEPSPs. The voltage responses were amplified using a Dagan BVC-700A amplifier (Dagan Corporation, Minneapolis, MN, USA), digitized using the ITC-18 board (Instrutech) on a PC using custom-made procedures in IgorPro (Wavemetrics, Lake Oswego, OR, USA). The electrical stimulus consisted of a single square waveform of 100 msec duration given at an intensity that generated 50% of the maximum fEPSP, using a stimulator equipped with a stimulus isolation unit (World Precision Instruments). Data were acquired and analyzed using custom-written procedures in IgorPro software (Wavemetrics). The voltage response was analyzed in order to measure the fEPSP slope. Baseline responses were monitored for at least 10 min.

For the LTP recordings, three theta-burst trains (5X4 spikes at 100Hz) with an inter-stimulus interval of 20 s were applied, whereas for the LFS-induced LTD recordings, 900 pulses

at 1Hz for 15min were applied. The fEPSPs were monitored for at least 50min following the end of each stimulation. The fEPSP slope of each response was normalized to the average 10 min pre-tetanic average fEPSP slope.

E.12. Quantification and statistical analysis

No samples or animals were excluded from analysis. Statistical analyses were performed with Microsoft Excel 2010 and GraphPad Prism 6 software. Mean, standard error of mean (± SEM) and statistical significance (pValue) were assessed by unpaired two-tailed Student's t-test or by ANOVA multiple comparisons. Statistical significance was established at pValue≤0,05.

F. Bibliography

Alvarez-Castelao, Beatriz, and Erin M. Schuman. 2015. "The Regulation of Synaptic Protein Turnover." *Journal of Biological Chemistry* 290(48): 28623–30.

Ascoli, Giorgio A. et al. 2008. "Petilla Terminology: Nomenclature of Features of GABAergic Interneurons of the Cerebral Cortex." *Nature Reviews Neuroscience* 9(7): 557–68.

Bateup, Helen S. et al. 2013. "Excitatory/Inhibitory Synaptic Imbalance Leads to Hippocampal Hyperexcitability in Mouse Models of Tuberous Sclerosis." *Neuron* 78(3): 510–22. http://dx.doi.org/10.1016/j.neuron.2013.03.017.

Caroni, Pico. 2015. "Inhibitory Microcircuit Modules in Hippocampal Learning." *Current Opinion in Neurobiology* 35: 66–73. http://dx.doi.org/10.1016/j.conb.2015.06.010.

Chu, Jianhua, and Stewart A. Anderson. 2015. "Development of Cortical Interneurons." *Neuropsychopharmacology* 40(1): 16–23. http://dx.doi.org/10.1038/npp.2014.171.

Eftekhari, Sanaz et al. 2014. "BDNF Modifies Hippocampal KCC2 and NKCC1 Expression in a Temporal Lobe Epilepsy Model." *Acta Neurobiologiae Experimentalis* 74(3): 276–87.

Flores, Carmen E., and Pablo MÃ©ndez. 2014. "Shaping Inhibition: Activity Dependent Structural Plasticity of GABAergic Synapses." *Frontiers in Cellular Neuroscience* 8(October): 1–13. http://journal.frontiersin.org/article/10.3389/fncel.2014.00327/abstract.

Fragkouli, A. et al. 2009. "LIM Homeodomain Transcription Factor-Dependent Specification of Bipotential MGE Progenitors into Cholinergic and GABAergic Striatal Interneurons." *Development* 136(22): 3841–51. http://dev.biologists.org/cgi/doi/10.1242/dev.038083.

Froemke, Robert C. 2015. "Plasticity of Cortical Excitatory-Inhibitory Balance." *Annual Review of Neuroscience* 38(1): 195–219. http://www.annualreviews.org/doi/10.1146/annurev-neuro-071714-034002.

Ganley, Ian G. et al. 2009. "ULK1·ATG13·FIP200 Complex Mediates MTOR Signaling and Is Essential for Autophagy." *Journal of Biological Chemistry* 284(18): 12297–305.

Gao, R, and P Penzes. 2015. "Common Mechanisms of Excitatory and Inhibitory Imbalance in Schizophrenia and Autism Spectrum Disorders." *Curr Mol Med* 15(2): 146–67. http://www.ncbi.nlm.nih.gov/pmc/articles/PMC4721588/pdf/nihms749865.pdf.

Gulyá, Attila I, Manuel Megías, Zsuzsa Emri, and Tamá F Freund. 1999. "Total Number and Ratio of Excitatory and Inhibitory Synapses Converging onto Single Interneurons of Different Types in the CA1 Area of the Rat Hippocampus." *The Journal of Neuroscience* 19(22): 10082–97.

Hara, Taichi et al. 2006. "Suppression of Basal Autophagy in Neural Cells Causes Neurodegenerative Disease in Mice." *Nature* 441(7095): 885–89.

Hayama, Tatsuya et al. 2013. "GABA Promotes the Competitive Selection of Dendritic Spines by Controlling Local Ca 2+ Signaling." *Nature Neuroscience* 16(10): 1409–16. http://dx.doi.org/10.1038/nn.3496.

Hu, Hua, Jian Gan, and Peter Jonas. 2014. "Fast-Spiking, Parvalbumin+ GABAergic Interneurons: From Cellular Design to Microcircuit Function." *Science* 345(6196).

Huang, X. et al. 2012. "Rapamycin Down-Regulates KCC2 Expression and Increases Seizure Susceptibility to Convulsants in Immature Rats." *Neuroscience* 219: 33–47. http://dx.doi.org/10.1016/j.neuroscience.2012.05.003.

Jung, Chang Hwa et al. 2010. "MTOR Regulation of Autophagy." *FEBS Letters* 584(7): 1287–95. http://dx.doi.org/10.1016/j.febslet.2010.01.017.

Kasai, Haruo et al. 2010. "Structural Dynamics of Dendritic Spines in Memory and Cognition."

Trends in Neurosciences 33(3): 121–29. http://dx.doi.org/10.1016/j.tins.2010.01.001.
Kelsom, Corey, and Wange Lu. 2013. "Development and Specification of GABAergic Cortical Interneurons." *Cell and Bioscience* 3(1): 1–19.
Kepecs, Adam, and Gordon Fishell. 2014. "Interneuron Cell Types: Fit to Form and Formed to Fit." *Nature* 505(7483): 318–26.
Kim, H. J. et al. 2017. "Deficient Autophagy in Microglia Impairs Synaptic Pruning and Causes Social Behavioral Defects." *Molecular Psychiatry* 22(11): 1576–84. http://dx.doi.org/10.1038/mp.2016.103.
Kim, Jeansok J., Joseph P. DeCola, Jesus Landeira-Fernandez, and Michael S. Fanselow. 1991. "N-Methyl-D-Aspartate Receptor Antagonist APV Blocks Acquisition but Not Expression of Fear Conditioning." *Behavioral Neuroscience* 105(1): 126–33.
Kim, Kook Hwan, and Myung Shik Lee. 2014. "Autophagy - A Key Player in Cellular and Body Metabolism." *Nature Reviews Endocrinology* 10(6): 322–37. http://dx.doi.org/10.1038/nrendo.2014.35.
Kins, Stefan, Heinrich Betz, and Joachim Kirsch. 2000. "Collybistin, a Newly Identified Brain-Specific GEF, Induces Submembrane Clustering of Gephyrin." *Nature Neuroscience* 3(1): 22–29.
Klausberger, Thomas, and Peter Somogyi. 2008. "Neuronal Diversity and The Unity Dynamics : Temporal Circuit Operations of Hippocampal." *Science (New York, N.Y.)* 321(5885): 53–57. http://www.ncbi.nlm.nih.gov/pubmed/18599766.
Komatsu, Masaaki et al. 2006. "Loss of Autophagy in the Central Nervous System Causes Neurodegeneration in Mice." *Nature* 441(7095): 880–84.
LaSarge, Candi L., and Steve C. Danzer. 2014. "Mechanisms Regulating Neuronal Excitability and Seizure Development Following MTOR Pathway Hyperactivation." *Frontiers in Molecular Neuroscience* 7(March): 1–15. http://journal.frontiersin.org/article/10.3389/fnmol.2014.00018/abstract.
Leonzino, Marianna et al. 2016. "The Timing of the Excitatory-to-Inhibitory GABA Switch Is Regulated by the Oxytocin Receptor via KCC2." *Cell Reports* 15(1): 96–103. http://dx.doi.org/10.1016/j.celrep.2016.03.013.
Liu, Guosong. 2004. "Local Structural Balance and Functional Interaction of Excitatory and Inhibitory Synapses in Hippocampal Dendrites." *Nature Neuroscience* 7(4): 373–79.
Marsden, W. N. 2013. "Synaptic Plasticity in Depression: Molecular, Cellular and Functional Correlates." *Progress in Neuro-Psychopharmacology and Biological Psychiatry* 43: 168–84. http://dx.doi.org/10.1016/j.pnpbp.2012.12.012.
Mills, Eric, Xian-ping Dong, Fudi Wang, and Haoxing Xu. 2010. "Mechanismis of Brain Iron Transport: Insight into Neurodegeneration and CNS Disorders." *Future Medicinal Chemistry* 2(1): 51–64.
Mizushima, Noboru, and Masaaki Komatsu. 2011. "Autophagy: Renovation of Cells and Tissues." *Cell* 147(4): 728–41. http://dx.doi.org/10.1016/j.cell.2011.10.026.
Mizushima, Noboru, Tamotsu Yoshimorim, and Beth Levine. 2010. "NIH Public Access." *Cell* 140(3): 313–26.
Morrison, R S et al. 1996. "Loss of the P53 Tumor Suppressor Gene Protects Neurons from Kainate-Induced Cell Death." *The Journal of neuroscience : the official journal of the Society for Neuroscience* 16(4): 1337–45. http://www.jneurosci.org/cgi/reprint/16/4/1337%5Cnpapers2://publication/uuid/016691CA-AE28-4230-9469-B18A78330D6A.

Nikoletopoulou, V., M. E. Papandreou, and N. Tavernarakis. 2015. "Autophagy in the Physiology and Pathology of the Central Nervous System." *Cell Death and Differentiation* 22(3): 398–407. http://dx.doi.org/10.1038/cdd.2014.204.

Nikoletopoulou, Vassiliki et al. 2017. "Modulation of Autophagy by BDNF Underlies Synaptic Plasticity." *Cell Metabolism* 26(1): 230–242.e5. http://dx.doi.org/10.1016/j.cmet.2017.06.005.

Nikoletopoulou, Vassiliki, and Nektarios Tavernarakis. 2018. "Regulation and Roles of Autophagy at Synapses." *Trends in Cell Biology* 28(8): 646–61. https://doi.org/10.1016/j.tcb.2018.03.006.

Portera-Cailliau, Carlos, David T Pan, and Rafael Yuste. 2003. "Activity-Regulated Dynamic Behavior of Early Dendritic Protrusions: Evidence for Different Types of Dendritic Filopodia." *The Journal of Neuroscience: The Official Journal of the Society for Neuroscience* 23(18): 7129–42. http://www.ncbi.nlm.nih.gov/pubmed/12904473%5Cnhttp://www.jneurosci.org/cgi/reprint/23/18/7129.

Rochefort, Nathalie L., and Arthur Konnerth. 2012. "Dendritic Spines: From Structure to in Vivo Function." *EMBO Reports* 13(8): 699–708. http://dx.doi.org/10.1038/embor.2012.102.

Sarkar, Sovan. 2013. "Regulation of Autophagy by MTOR-Dependent and MTOR-Independent Pathways: Autophagy Dysfunction in Neurodegenerative Diseases and Therapeutic Application of Autophagy Enhancers." *Biochemical Society Transactions* 41(5): 1103–30. http://biochemsoctrans.org/lookup/doi/10.1042/BST20130134.

Seglen, P O, and P Bohley. 1992. "Autophagy and Other Vacuolar Protein Degradation Mechanisms." *Cellular and Molecular Life Sciences* 48(2): 158–72. http://dx.doi.org/10.1007/BF01923509.

Tang, Guomei et al. 2014. "Loss of MTOR-Dependent Macroautophagy Causes Autistic-like Synaptic Pruning Deficits." *Neuron* 83(5): 1131–43. http://dx.doi.org/10.1016/j.neuron.2014.07.040.

Tremblay, Robin, Soohyun Lee, and Bernardo Rudy. 2017. "Properties To Circuits." 91(2): 260–92.

Tricoire, Ludovic et al. 2012. "NIH Public Access." 31(30): 10948–70.